Characterisation of naturally occurring radioactive materials in the Mozambique-to-Secunda gas pipeline

TR Leeuw

orcid.org/0000-0002-6179-6116

Dissertation accepted in fulfilment of the requirements for the degree *Master of Science in Engineering Sciences with Nuclear Engineering* at the North-West University

Supervisor:	Prof MV Tshivhase
Assistant-supervisor:	Mr TC Dlamini

Graduation:	November 2022
Student number:	21940916

Acknowledgements

I am grateful to the Lord God for giving me the strength and courage to continue working hard. It has not been easy to stay awake at night and do the research. I also want to thank my wife for giving me the support and space to complete this work.

I would also like to thank Prof Victor Tshivhase for believing in the importance of this work and agreeing to supervise me and Dr Thulani Dlamini for his guidance and co-supervision. Dr Dlamini has been patient and willing to make research challenging and exciting for me. His in-depth knowledge of the HPGe spectrometer has contributed vastly to the success of this work. My gratitude goes to the PhD students Vaino Indongo and Dikeledi Mokhene who have been a constant support during the running of the samples and analysis of the spectrum. Thanks to the entire staff at CAST including Tsholofelo Mokgele, the Lab Technician for making sure everybody had a chance to run their counting, Monde Kakula for making sure the nitrogen bottles were always full during the difficult times of the Covid-19 pandemic and the cleaning staff for making sure the facility was kept clean.

I.

Abstract

Title: Characterising and quantifying NORM in waste from the Mozambique to Secunda Gas Pipeline cleaning

Author: Tlamelo R Leeuw

Supervisor: Prof. V Tshivhase

Co-supervisor: Dr T Dlamini

Internationally all oil and gas extraction and processing operations are required by authorities to monitor and report on accumulation of naturally occurring radioactive material, NORM, and technically enhanced naturally occurring radioactive material, TENORM (IOGP, 2016a). This is necessary because workers and the environment will be exposed to ionising radiation from TENORM during maintenance and operations when radioactive solid waste and liquid waste from these operations are to be disposed. Table below shows different radiological risks to the workers and members of the public.

Comparison of radiological risks for this study with other countries

Country	Ra_{eq} (Bq/kg)	D_γ (nGy/h)	D_{eff} (mSv/y)
This study	**2.17-8.98**	**2.45-4.06**	**3.01-4.98**
Saudi Arabia	21.6 - 204	10.5 - 96.4	0.013 - 0.118
Egypt	544 - 596	250 - 273	306 - 335
Tunisia	0.09 - 398	0.043 - 177	5.28×10^{-5} - 3.64×10^{-4}
Algeria		$(0.1 - 100) \times 10^3$	0.01 - 0.6
Nigeria	51.04 - 100.85	23 - 47	0.027 - 0.057
Congo	-	$(0.1 - 6) \times 10^3$	-
Italy	-	$(0.1 - 6) \times 10^3$	-
Ghana	-	10 - 57	12.6 - 83.4
USA	-	-	0.002 - 0.5

Based on the maximum radium equivalent of 8,98 Bq/kg from this study it is concluded that members of the public are not exposed to harmful radiation. The radiation is far less than the 1 mSv/y which is the recommended limit for members of the public. The

estimation of potential radiological risks based on radium equivilent, absorbed dose rate, annual effetive dose equivalent, hazard indices and estimated lifetime cancer risk shows that the workers and members of the public are not exposed to deterministic and stochastic health effects by being exposed to these levels of radiation.

It is recommended that this type of work must be done throughout the entire gas value chain starting from gas fields. Although the radiation activity concentration is low, the current commitment to strict safety procedures and high standards of protection of the public and environment be maintained.

Keywords:

Activity, dose, cancer, environment, hazards, lifetime, nuclides, public, radiation, workers

I.

Table of contents

I.

List of figures

I.

List of tables

Definition of terms

All definition of terms and other definitions are as stated in Lamarsh (2001) and as per referenced authors.

Table 1: List of abbreviations and acronyms

AEDE	Annual effective dose equivalent
CNG	Compressed natural gas
ELCR	estimated lifetime cancer risk
HIH	Heritable Ill Health
HPGe	High purity germanium spectroscopy
IAEA	International Atomic Energy Agency
IOGP	International Association of Oil and Gas Producers
K	Potassium
LNG	Liquefied natural gas
MDA	Minimum detectable activity
MSP	Mozambique Secunda Pipeline
NORM	Naturally occurring radioactive material
NWU	North-West University
OECD	Organisation for Economic Co-operation and Development
pig	a pipeline scraping device to remove scale and for determining pipeline integrity
PPE	Personal protective equipment
RRC	Risk of Radiation-related Cancer
Redox	Reduction-oxidation
ROMPCO	Republic of Mozambique Pipeline Company
STS	Scraper station
TEG	Triethylene glycol, used to de-hydrate gas
TENORM	Technically enhanced naturally occurring radioactive material
Th	thorium
U	uranium
UNSCEAR	United Nations Scientific Committee on effects of atomic radiation

1 Introduction

1.1 Background and problem statement

Internationally all oil and gas extraction and processing operations are required by authorities to monitor and report on accumulation of naturally occurring radiation material, NORM, and technically enhanced naturally occurring radiation material, TENORM (IOGP, 2016a). This is necessary because workers and the environment will be exposed to ionising radiation from NORM and TENORM during maintenance and operations when radioactive solid waste and liquid waste from these operations are to be disposed. Different institutions in the world have investigated NORM concentrations at different oil and gas fields. Table 2 shows typical TENORM concentration ranges of scale in oil and gas. The scale comes from equipment and pipelines transporting oil and gas.

Table 2: Showing typical ranges of the NORM in scales in the oil and gas industry from different regions (Ali et al., 2019)

Country	^{238}U Bq/kg	^{232}Th Bq/kg	^{40}K Bq/kg	^{226}Ra Bq/kg
Algeria	-	-	-	0.001 - 0.95
Congo	0.9 - 2.7	0.8 - 2.2	-	97 - 151
Egypt	9140 - 285 823	427 -34 339	51 - 1031	-
Ghana	-	16.9 - 40	42.65 - 44.05	28.22 - 47.54
Sudan	358.05 - 4106.9	375.88 - 2736.7	16.05 - 9294	-
Tunisia	0.9 - 7.6	0.8 - 5.1	31 - 1189	-
Saudi Arabia	< LD	0.14 - 3.1	4.3 - 9.6	0.8 - 1.5
UK	0.94 - 5.17	0.18 - 0.86	-	58.8 - 131.6
Italia	0.9 - 53.8	0.8 - 18.9	-	2.7 - 1126

These analysis are done regularly to update databases of NORM in different oil and gas industry products from different regions of the world. The information is used in taking precautionary measures to protect workers and environment in oil and gas industry against ionising radiation. Typical data is shown in Table 3.

Table 3: Shows typical concentrations of TENORM in the crude oil and natural gas (Ali et al., 2019)

Radio Isotope	Crude oil Bq/kg	Natural gas Bq/kg
^{238}U	0.0001 - 10	-
^{232}Th	0.3 - 2	-
^{226}Ra	0.1 - 40	-
^{228}Ra	3 - 17	-
$^{222}R\text{-}n$	0.05 - 301	5 - 200 000
^{210}Pb	-	0.005 - 0.02
^{210}Po	0 - 10	0.002 - 0.08

There is a scheduled maintenance plan to regularly clean and inspect the pipeline from Temane in Mozambique, to Secunda in South Africa. Radioactive solid waste from previous cleaning and inspection campaigns has been accumulated in Komatipoort South Africa waiting to be disposed. This waste must be analysed in order to be safely disposed.

1.2 Objectives and structure of the thesis

The purpose of this research is to characterise and quantify the radioactive waste for safe storage and disposal.

The objectives of the study are to:

1. Characterise the radioactive nuclides as follows:
    a. Identification of the radioactive nuclides
    b. Determine individual nuclide activity concentration
2. Estimate the potential radiological risk due to exposure to the NORM in the scale waste

3. Future work

The thesis consists of the following chapters:

1. **Introduction** which includes a brief background of NORM in the oil and gas industry and associated concentrations in waste and in crude oil and gas.

2. **Literature review** survey gives an overview of natural gas transportation and cleaning of pipelines from where waste in the form of scale is derived. The basis is laid for the scientific theory and equations that will be used to meet the objectives.

3. **Methods** which are based on the theoratical basis discussed in literature review and equations treated in the literature. Sampling procedures and sample analysis methods are discussed.

4. **Results and discussions** of study based on the theoretical work discussed in literature survey. This includes the demonstration of the originality of the author's contribution.

5. **Conclusions and recommendations**

6. **Literature** review

2 Literature review

2.1 Oil and gas pipeline operation

The oil and gas value chain starts with the extraction of oil and gas from underground. The extracted oil and gas are then refined and processed at the extraction site or are refined and processed into various products at remote sites. After refining and processing they are stored ready for transportation to various market destinations. This study focuses on the radioactivity related to the operation and maintenance of the natural gas transportation pipelines.

2.1.1 Transportation of natural gas

Transportation of natural gas depends amongst other factors on distance and end use. Below are three of the most widely used methods of transporting natural gas (Nikolaou, 2013).

2.1.1.1 Compressed natural gas, CNG, transportation

Natural gas can be compressed to pressure of 250-300bar in tube bundles for transportation. The pressurised tube bundles are loaded on the ship in racks. The compression ratio is 300:1 (Nikolaou et al., 2009). As aresult the important tube construction parameters are geometry, tube material and pressure. The temperature of the gas remains ambient while pressure is the parameter that is manipulated to achieve the required compression ratio.

This method of transportation is preferred when transporting stranded gas from remote locations. The gas is then released into onshore pipeline network. Lately the racks packed with compressed natural gas in tubes are loaded on trucks to be offloaded to site where the gas will be utilised such as refuelling trucks and cars that run on compressed natural gas.

2.1.1.2 Liquefied natural gas, LNG, transportation

Natural gas can also be liquefied to reduce its volume and hence make it easier for transportation. In the case of LNG temperature is the manipulated parameter. The gas is cryogenically cooled down to temperature of -160^0C (Mokhatab, 2018). It changes phase from gas to liquid and can thus be stored in a vessel with much

smaller volume for transportation. The volume reduces to 1/600th (Nikolaou et al., 2009) of original volume.

This method is preferred for transporting natural gas offshore over long distances on the sea and requiring large volumes. At the destination port the gas will be gasified and released into the onshore pipeline network.

2.1.1.3 Transportation of natural gas in pipelines

Natural gas can be transported by pipelines onshore within a country or across several countries. This is the most efficient and economic way of transporting natural gas over long distances from processing facilities to end users. For this to be economic the pipelines inner diameter, ID, must be large. Typical diameters range from more than 0,66m to 1.2m (Folga, 2007). The pipelines are normally made of carbon steel and the wall thickness depends on natural gas pressure. They are also coated with epoxy to protect them from corrosion caused by underground moisture and rust. Cathodic protection, which is application of light current through the pipe, is also used to prevent corrosion. Corrosion monitoring coupons are inserted in areas where the risk of corrosion is high.

Apart from transporting natural gas, the pipelines also act as natural gas storage facility. The pipeline will be pressurised with natural gas, also called packing with natural gas, to pressure typically greater than 35bar (Folga, 2007). Compressors are installed along the pipeline in order to maintain the pressure and the packing. Normally at the compressor station there will be a scraper station where the pipe cleaning devices will be received and launched. Filters are installed just before the compressors to remove dust which could damage compressor blades. Operation and maintenance of these compressor stations means personnel will be regularly exposed to radioactive waste.

Radiation related to transportation of natural gas with pipelines is the focus of this study.

2.1.2 Pipeline cleaning

In the oil and gas industry sediments and deposits interfere with the flow of natural gas in the pipeline. It is therefore crucial to do pipeline cleaning regularly. It is also necessary for oil and gas operators to clean the pipelines in order to do integrity checks and statutory maintenance. Therefore the pipelines are designed with scrapper stations and injection systems where cleaning devices can be inserted (van der Werff and BV, 2006) and (Wang and Sun, 2015). There are different methods for pipeline cleaning. Oil and natural gas pipelines can be cleansed by flushing, chemical cleaning and pigging and with other methods which will not be touched in this study.

2.1.2.1 Flushing of natural gas pipelines

Pipelines can be flushed with water or steam from injection systems. Water and gas can be combined to create a larger shear stress at the interface with the deposits. The loose scale will be removed from the walls of the pipeline and be flushed with the flushing medium to the collection point. This method is not used for long pipelines running across the country or across the continent such as in Europe and North America. Large volumes of water will be required and large amounts of steam will be needed at high enough pressure. Besides the large volumes of flushing medium required, the disposal of this dirt and scale containing medium will cause environmental concerns. This method is only used for short distances.

2.1.2.2 Chemical cleaning of natural gas pipelines

There has been a development of chemical agents with unique physical properties for the cleaning of pipelines (van der Werff and BV, 2006). The key factor also being environmentally friendly and safe for handling by workers involved in the pipeline cleaning. The chemical agents contain biodegradable surfactants which makes them environmentally friendly. However, natural gas transporting pipelines are large diameter pipelines running for long distances. It is therefore uneconomic to clean the entire pipeline or long section of the pipeline with chemical agents. This method is only used for small sections where other methods of cleaning have not been successful.

2.1.2.3 Pigging of natural gas pipelines

The most popular pipeline cleaning method in oil and gas industry large and long pipelines is by inserting a device called a "pig". This device derives its name from the sound it makes as it moves inside the pipeline. It sounds like a crying pig. A back-acronym, **p**ipeline **i**nspection **g**auge, has been created to fit the name pig. There are several types of pigs but this study will confine itself to 2 types relevant to this investigation (van der Werff and BV, 2006) and (Wang and Sun, 2015).

2.1.2.3.1 Cleaning pig

The cleaning pig is a devise fitted with scraping brushes (Wang and Sun, 2015). Aloso see Figure 1. As the pig moves inside the pipeline the brush removes scale from the inside walls of the pipeline and loosens hard scale. A second pig with different brushes may be inserted to remove loosened scale.

Figure 1**:** A cleaning/scraping pig with wire brushes EPCM (2021)

The pig is inserted at a pig-launching station using a pig-launcher. The pig-launcher is fitted with isolation valves for safe launching into the process stream, natural gas in this case as shown on Figure 2. The pig is pushed forward by the flowing natural gas without disturbing transportation of gas.

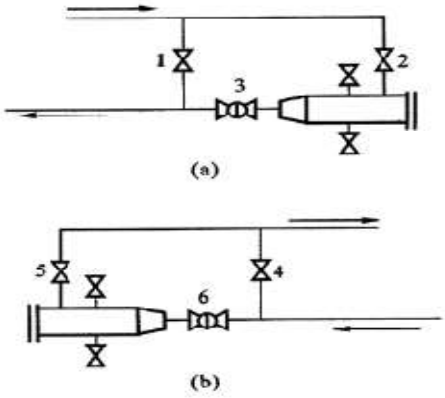

Figure 2**:** The flow diagram of a pig (a) launcher and (b) receiver (Wang and Sun, 2015)

The scale removed from the walls of the pipeline is also pushed forward by the second pig and the gas. The accumulated scale together with the pig is received on the other end at the pig receiving station called the pig-receiver. Similar to the pig-launcher the pig-receiver is also fitted with isolation valves for safe operation. The scale, which has become fine dust by now, is collected in drums by personnel wearing appropriate PPE for radioactive waste. The drums are then sealed, marked and stored.

2.1.2.3.2 Intelligent pig

The intelligent pig is fitted with electronic devices for inspection of the integrity of the pipeline. See Figure 3 below. It records wall thickness, presence of corrosion and erosion and maps the geometry of the pipeline. It will push the remaining scale forward although this is not the intended purpose. It is launched and received similar to the scraping pig.

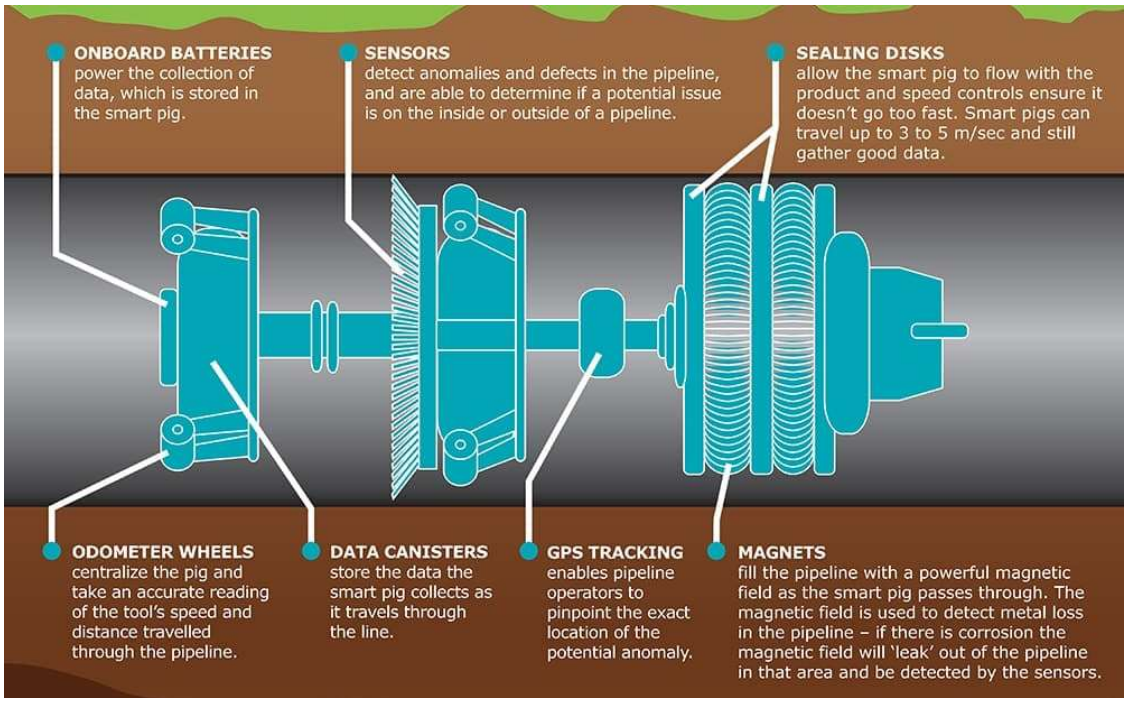

Figure 3 An intelligent pig fitted with electronic devices, CAPP (2018)

2.2 Radioactive waste from pipeline cleaning

2.2.1 Liquid and slurry waste

Radioactive liquid waste in oil and gas industry is in the form of process water. This only occurs at the gas processing facility. Water is removed from natural gas by contacting the gas with TEG. The removal of water is to ensure that there is no water present when the gas is chilled. This is to prevent formation of hydrates in the chiller. The gas is further chilled to a dew point temperature of -6.8^{0}C at 625 kPa(g) by heat exchanging with cold propane which undergoes compression and expansion and hence temperature reduction due to Joule Thompson effect. Under these conditions the gas is considered to be dry. The drying of the gas is to ensure that there is no oil or liquids entering the compressors. Therefore past the compressors there will be no liquid or slurry waste from the cleaning of pipelines. Liquid waste would come from flushing pipelines with water or chemical mixture. This is normally not done for pipelines running across the country.

2.2.2 Scale

Scale forms in the inner surface of the pipe. The scale can grow to the point where the inner diameter of the pipe is reduced and the pathway for the gas is smaller. This creates a high pressure drop and less gas is transported or stored. NORM is found as impurities as shown in Table 4. It co-precipitates or deposits with other chemical elements having similar properties. For example ^{226}Ra and ^{228}Ra are chemically similar to Ba, Sr, Ca, and Mg. In oil and gas facilities the most common types of scale are sulphates and carbonates such as $BaSO_4$ and $CaCO_3$ (Attallah, 2012). Traces of ^{226}Ra and ^{228}Ra will be found in these scales. The use of scale inhibitors also assists in minimising NORM deposits.

The rates and amounts of scale and NORM deposition depend on operating conditions. According to Attallah (2012) changes in the following operating conditions can lead to accumulation of NORM.

- Change in temperature and pressure
- pH
- Changes in flow patterns (laminar and turbulent flow) and
- gas expansion

Table 4 NORM activity concentration range for scale and deposits (IOGP, 2016a)

	NORM	Bq[Norm]/kg[scale] x10^3	Bq[Norm]/kg[deposit] x10^3
^{232}Th	^{232}Th	1.0- 2.0	0.001 - 0.07
	$^{228}Ra_{eq}$	50.0 - 2800	0.05 - 300
^{238}U	$^{238}U_{eq}$	0.001 - 0.5	0.001 - 0.05
	$^{226}Ra_{eq}$	0.1 - 15000	0.8 - 400
	$^{210}Pb_{eq}$	0.02 - 75	0.05 - 2000

2.3 Radioactivity in the oil and natural gas industry

Most of the potassium, uranium and thorium found in oil and gas comes from minerals deposited in rocks and in sandstone. In these original forms underground these radioactive material pose no danger to human beings. During gas and oil

extraction these NORM are disturbed and brought above surface with oil, gas and associated water and they become a health hazard to personnel.

In the 1980's higher levels of NORM were detected in oil and gas equipment used in the North Sea drilling operations (Pataki and Cahill, 1999). Subsequently, these were also detected in other parts of the world where oil and gas operations were taking place (Ali et al., 2019). The most significant NORM found were ^{40}K, ^{232}Th and ^{238}U. They undergo natural radioactive decay by emitting alpha-particles and beta-particles accompanied by emission of gamma-photons. The decay leads to the production of other radioactive nuclides referred to as daughter nuclides such as radon and radium (Zielinski and Otton, 1999)

In 1990 the New York State Department of Environmental Conservation performed studies to determine if there were higher concentrations of NORM at the New York State oil and gas wells (Pataki and Cahill, 1999). Results showed concentrations no more than twice the background values. In 1994 the same was found by the State of Pennsylvania when analysing waste from oil and gas wells. However, in 1996 the New York State carried more investigations but this time including samples from more oil and gas wells. Results showed scale concentration of ^{226}Ra ranging from none detected to 400 Bq/kg.

The radioactive nuclides pose no danger in their natural form when they are left undisturbed in the earth's crust. However, when oil and gas are extracted from underground, the NORM are concentrated to higher concentration levels and extracted with the oil, gas and associated water with their daughter nuclides. In this form they are referred to as technologically enhanced naturally occurring radioactive materials, TENORM. Figure 4 below shows different deposits of oil and gas.

Depending on methods of extraction they could be enhanced to concentrations that are harmful to human beings and the environment when brought above surface. They will concentrate in pipes, equipment and waste above surface far from where they naturally occur underground. They become a health, safety and environmental hazard (Pataki and Cahill, 1999)

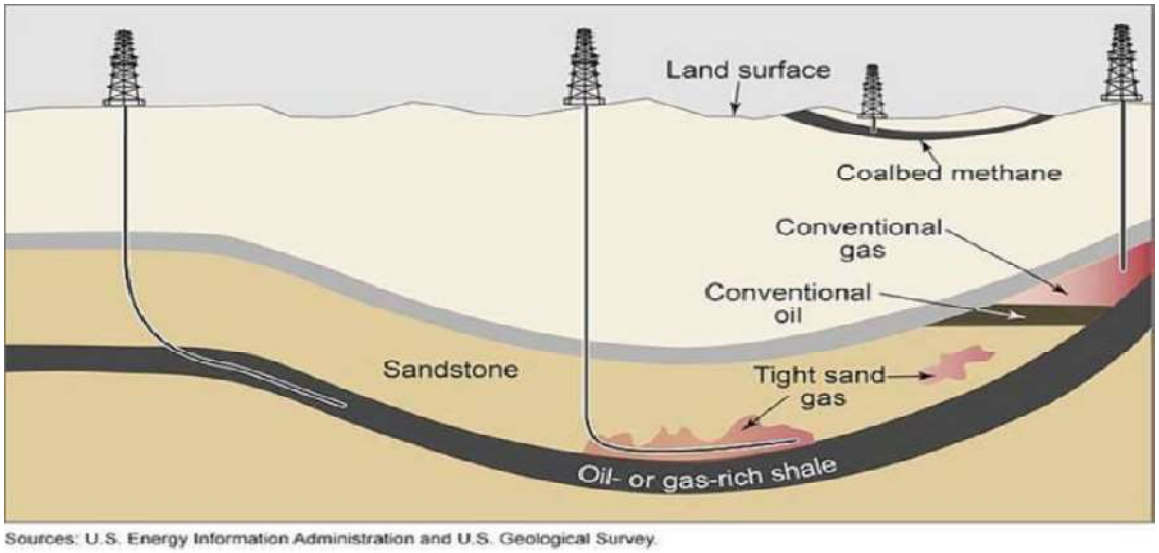

Figure 4: Different types of oil and gas extraction (Thompson, 2015)

Analysis has been conducted internationally to give mean and range abundances of potassium, thorium and uranium in sedimentary rocks shown in Table 5 (IOGP, 2016a)

Table 5: Shows the mean and range of potassium, thorium and uranium in sedimentary rocks (IOGP, 2016a)

Sedimentary Rock Class	uranium (U)			thorium (Th)			potassium (K)		
	ppm		Bq/kg	ppm		Bq/kg	%		Bq/kg
	mean	range	mean	mean	range	mean	mean	range	mean
			$x10^3$			$x10^3$			$x10^3$
Sandstone	4.1	0.1 - 62	0.05	9.7	0.7 - 227	0.04	1.2	0.1 - 8.5	0.4
Shale	5.9	0.9 - 80	0.07	16.3	5.3 - 39	0.07	3.5	0.9 - 8.5	1.1
Clay	4	1.1 - 16	0.05	8.6	1.9 - 55	0.03	0.6	0.1 - 2.6	0.2
Chemical	3.6	0.03 - 27	0.04	14.9	0.03 - 132	0.06	0.6	0.02 - 8.4	0.2
Carbonates Limestone	2	0.03 - 18	0.02	1.8	0 - 11	0.007	0.3	0.01 - 3.5	0.09

2.4 NORM and TENORM

2.4.1 Radioactivity

NORM emits high energy charged alpha- and beta-particles accompanied by release of high energy ionizing gamma-photons (IOGP, 2016a).

2.4.1.1 Alpha-Particles:

Alpha particles are positively charged heavy mass particles. An alpha particle consists of 2 protons and 2 neutrons and is denoted as α or ^{4}He. They are emitted due to repulsive Columbic electromagnetic forces of protons repelling each other in the nucleus of unstable elements. The release of an α-particle can be represented as follows

$$ {}^{A}_{Z}X_{\mathrm{N}} \underset{\alpha}{\rightarrow} {}^{A-4}_{Z-2}X_{\mathrm{N}-2} + {}^{4}_{2}\alpha $$

They lose energy very quickly and as a result only travel less than 10μm in solid matter. They cannot penetrate outer tissue of skin as shown on Figure 5. The energies of emitted alpha-particles range from 4MeV to 7Mev (Jevremovic, 2009). The half-lives of elements emitting alpha particles range from microseconds to 10^{17} and depend on the energy of the emitted alpha-particle.

Based on the law of conservation of energy, the energy released when an alpha particle is emitted is given by the following relation (Santawamaitre, 2012)

$$ Q = E_d + E_\alpha \qquad (1) $$

Where E_d and E_α are kinetic energies of the daughter nuclide and the alpha-particle respectively

Therefore;

$$ Q = \frac{1}{2}(m_\mathrm{d} v_d^2 + m_\alpha v_\alpha^2) \qquad (2) $$

Based on the law of conservation of momentum the following relation applies;

$$ m_d v_d = m_\alpha v_\alpha \qquad (3) $$

It can also be shown that

$$ \frac{E_d}{E_\alpha} = \frac{m_\alpha}{m_\mathrm{d}} \qquad (4) $$

From equations 1 and 4

$$E_{\alpha} = \frac{Q}{\left(1 + \frac{m_{\alpha}}{m_{d}}\right)} \quad (5)$$

Therefore the energy of the emitted alpha-particle can be calculated from the energy released from the emission, mass of the daughter nuclides and the mass of the alpha-particle.

The energy of the released alpha-particle can also be calculated from the Geiger-Nuttall law (Van Rooyen, 2021)

$$log_{10}\lambda = a_1 \left(\frac{Z}{\sqrt{E}}\right) + a_2 \quad (6)$$

Based on the values of a_1 and a_2 as given by Van Rooyen (2012) the following relation can be obtained;

$$E_{\alpha}(Z,T) = \frac{1.426712931Z^2}{(0.434294482ln\left(\frac{ln2}{T_{\frac{1}{2}}}\right) - 36.324957928)^2} \quad (7)$$

It should be noted that this formula has been derived empirically and not from fundamental principles (Van Rooyen, 2012). The equation can be used with confidence under the following conditions:

$E_{\alpha} \in [3.5; 8.7]\ MeV$

$T_{\frac{1}{2}} \in [10^{-2}s;\ 10^{11}yr]$

2.4.1.2 Beta-Particles:

Beta particles are charged particles originating from the nucleus and have high energy and very small mass. At the energy level of 500keV they can travel 1mm in tissue. As a result, they can cause harm to living cells. They can be shielded with aluminium or steel as depicted by Figure 5. However, they cannot be shielded with ordinary PPE such as overalls and gloves. There are two types of beta-particles, an electron and a positron. An electron is formed when a neutron in an unstable nucleus decays into a proton,

$n \rightarrow p + e^{-} + V_e$

The energy released when electron is emitted is given by the following equation (Lieser, 1997)

$$\Delta E = (m_p - m_{\mathrm{d}} - m_e)c^2 \quad (8)$$

Where m_p,m_{d}, and m_e are mass of parent nuclide, mass of daughter nuclide and mass of electron respectively. The mass of the nuclide is given by the mass of the nucleus plus the electron as follows

$$M = m + Zm_e \quad (9)$$

This implies that;

$$m = M - Zm_e \quad (10)$$

Substitute equation 10 in equation 8 and simplifying gives;

$$\Delta E = (M_p - M_d)c^2 \quad (11)$$

Positrons are formed when protons in an unstable nucleus decays into a neutron.

$p \rightarrow n + e^{+} + V_e$

Similar to the electron, the energy released by the positron is given by, (Lieser, 1997)

$$\Delta E = (M_p - M_d - 2m_e)c^2 \quad (12)$$

Empirical formulae have been developed for beta-particle emissions similar to alpha-particle emissions (Lieser, 1997).

$$log_{10}\lambda = a_1 + a_2 log_{10}E_{max} \quad (13)$$

2.4.1.3 Gamma-photons:

Gamma ionising photons are neutral and normally accompany release of alpha-particles and beta-particles. They travel indefinite distances in air and can only be stopped by high electron density elements such as Pb as shown on Figure 5. They will ionise internal human tissues that interact with them and are therefore a hazard to human beings. Gamma-photons are released when an unstable nucleus rearranges its protons and neutrons in order to be stable. In the process high energy

photons are released. The recoil energy is normally very small such that the change in energy is practically the gamma-photon energy (Lieser, 1997)

$$\Delta E = E_\gamma \quad (14)$$

Gamma-rays have well defined energies. This property is utilised in gamma-spectroscopy. The excited nucleus may transmit its energy to an electron in the K-shell instead of emitting a gamma-photon. This process is called internal conversion, IC. In this case an internal conversion electron is released instead of a gamma-photon and its energy is given by;

$$E_e = E_\gamma - E_B \quad (15)$$

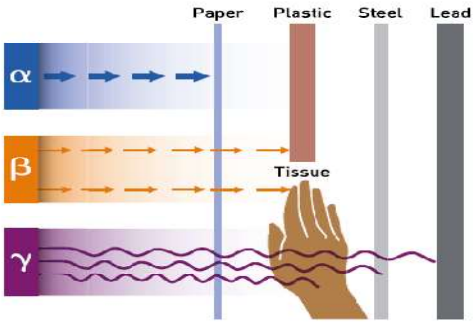

Figure 5: enetration and shielding of ionising radiation IOGP (IOGP, 2016a)

2.4.2 Sources of NORM

According to Ahmed (2007) NORM originates from three types of sources. These are cosmic, terestrial and internal. This investigation will only focus on terrestrial sources.

The earth's crust contains all naturally existing elements of the periodic table. Only 8 of them make up 98.5%. These are oxygen, silicon, aluminium, iron, calcium, sodium, magnesium and potassium IOGP (IOGP, 2016a). Naturally occurring radioactive materials, NORM, such as ^{40}K, ^{232}Th and ^{238}U, can also be found occurring naturally in the earth's crust in varying concentrations. Abundance of ^{40}K in the earth's crust is 2.1% whereas thorium and uranium's abundance is in parts per million. They are recorded as existing from more than 4 billion years ago and are referred to as primordial radioactive material. This means they were generated by stellar processes of the universe. They are found in minerals such as apatite, sphene, zircon, allanite, monazite, pyrochlore, thorite and xenotime.

Hazen et al. (2009) states that the formation of these minerals occurred over 4 phases. The first phase happened around 4.5 billion years when thorium and uranium in magmatic-related fluids precipitated in the crust. These are Th^{4+} and U^{4+} minerals such as thoriumite, ThO_2, uranimite, UO_2, and coffinite, $USiO_4$. The second phase occurred from around 3.4 billion years with the formation of detrital uranimite with some thorium. These minerals are found in the Witwatersrand. Limited amounts of uranyl oxide-hydroxides are also found. The 3rd phase involves formation of most uranium minerals. They precipitated from saline solutions at 100°C to 300°C carrying$(UO_2)^{+2}$-chloride complexes. They contain low amounts of thorium and are found in Australia, Canada and Ghana. The 4th phase started around 400 million years ago. Redox reactions occurred as a result of multiple oxidation states of $U(^{+2,+4\ and+6})$. Thorium is found in very low amounts unless there are aqueous solutions that promote solubility of thorium. The 4th phase promoted sandstone-type ore deposits.

2.4.3 Decay Series

2.4.3.1 Thorium decay Series

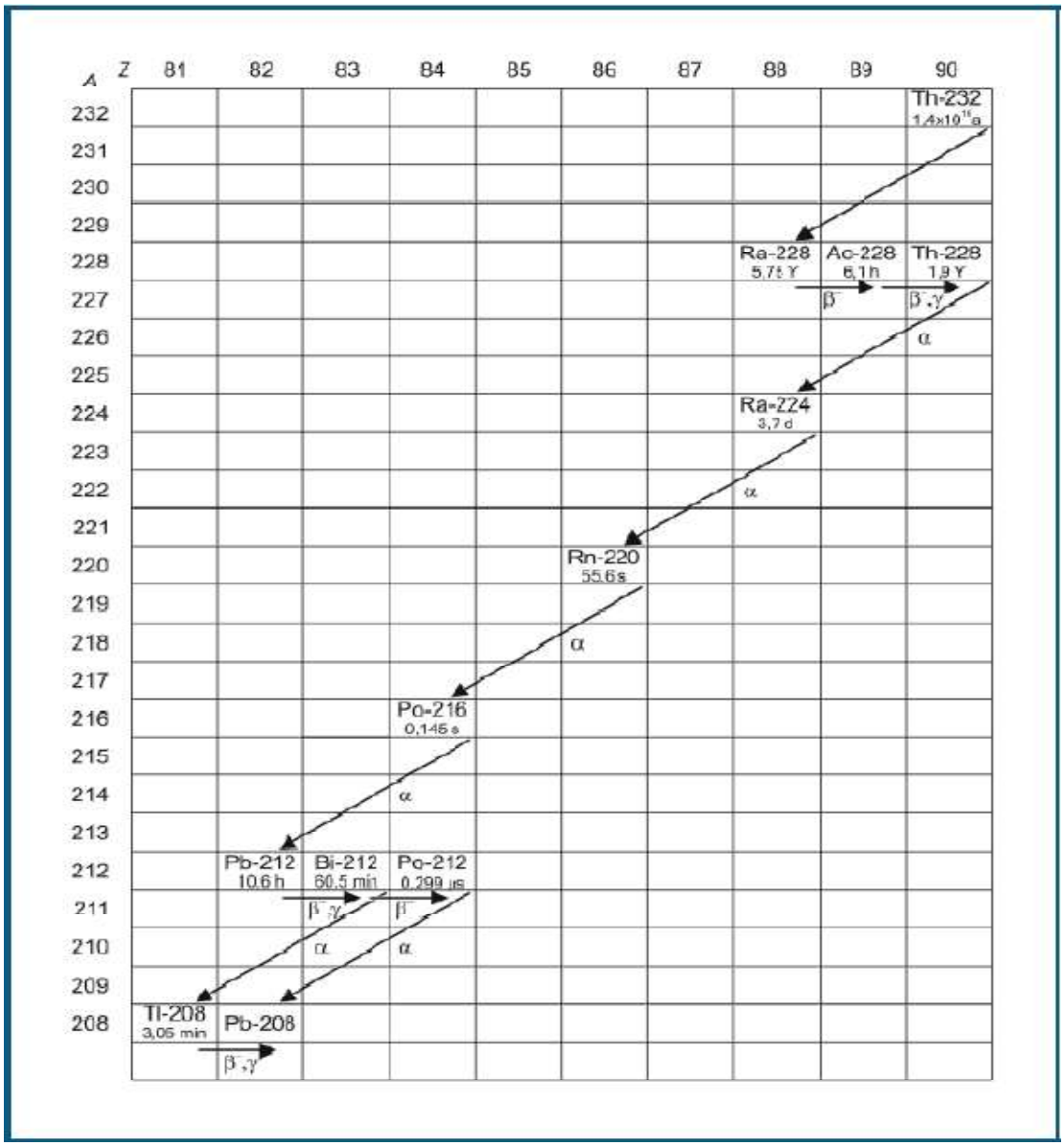

Figure 6: Decay series of thorium with its daughter nuclide

The thorium decay series is shown on Figure 6. The mass number of isotopes in the thorium decay series can be represented as 4n. This decay series starts with the unstable radioactive ^{232}Th and ends with the stable isotope ^{208}Pb. Figure 6 above shows the release of alpha- and beta-particles. The half-life of ^{232}Th is recorded as 13.9 billion years.

It should be noted that gamma-photons are also release at different energy levels by some isotopes. At the energy level of 911 keV, ^{226}Ac releases gamma-photons when decaying to ^{228}Th. The intensity of this release is 25%. This is followed by ^{212}Pb decaying to ^{212}Bi at 238.6 keV. The intensity is 43%. Higher intensities are exhibited by ^{208}Ti decaying to ^{208}Pb at 583 keV and 2614 keV. Peaks at these energy level are important in identifying the presence and activity of thorium with its daughter nuclides. The different energy levels are shown in Table 6

Th-232 Ingrowth

In the ^{232}Th decay series, ^{228}Ra has the longest half-life. It will take about 8 x T1/2 of ^{228}Ra to grow in and reach near equilibrium (Van Rooyen, 2012). It will take about 8 x 5.6 million years to grow in and reach near equilibrium. At this stage of near full equilibrium the photon yield is 4.1384. Different daughter nuclides have yields at different energies as shown in Table 6. These photon lines are unique to ^{232}Th.

Table 6: Energy and Yield lines that are indicative of the presence of ^{232}Th in a sample (Van Rooyen, 2012)

^{232}Th	
Photon Energy MeV	Photon Emission Yield
0.23863	0.43461
2.61453	0.35761
0.58319	0.30469
0.91120	0.25754
0.07741	0.17789
0.96897	0.15772
0.01628	0.13267
0.01298	0.11653
0.33832	0.11250
0.07506	0.10638

0.01620	0.08983
0.51077	0.08154
0.72733	0.06604
0.01084	0.06230
0.00307	0.05619
0.96477	0.04981
0.86056	0.04481
0.46300	0.04392
0.79495	0.04242
0.24099	0.04115

Contribution of photons where ^{232}Th is at equilibrium with its daughter nuclides comes mainly from ^{228}Ac (40.229%) and ^{208}Ti (46.055%). This is shown as % contribution in Table 7.

Table 7: Showing the contribution of the individual daughter nuclide in the ^{232}Th decay series to the effective dose rate around an unshielded point-like source of ^{232}Th at equilibrium with its daughter nuclide (Van Rooyen, 2012)

Nuclide	% Contribution to Photon DR
^{232}Th	0.128
^{228}Ra	0.274
^{226}Ac	40.229
^{228}Th	0.251
^{224}Ra	0.538
^{220}Rn	0.032
^{216}Po	0.001
^{212}Pb	7.684
^{212}Bi	4.81
^{212}Po	0
^{208}Ti	46.055

2.4.3.2 Uranium decay Series

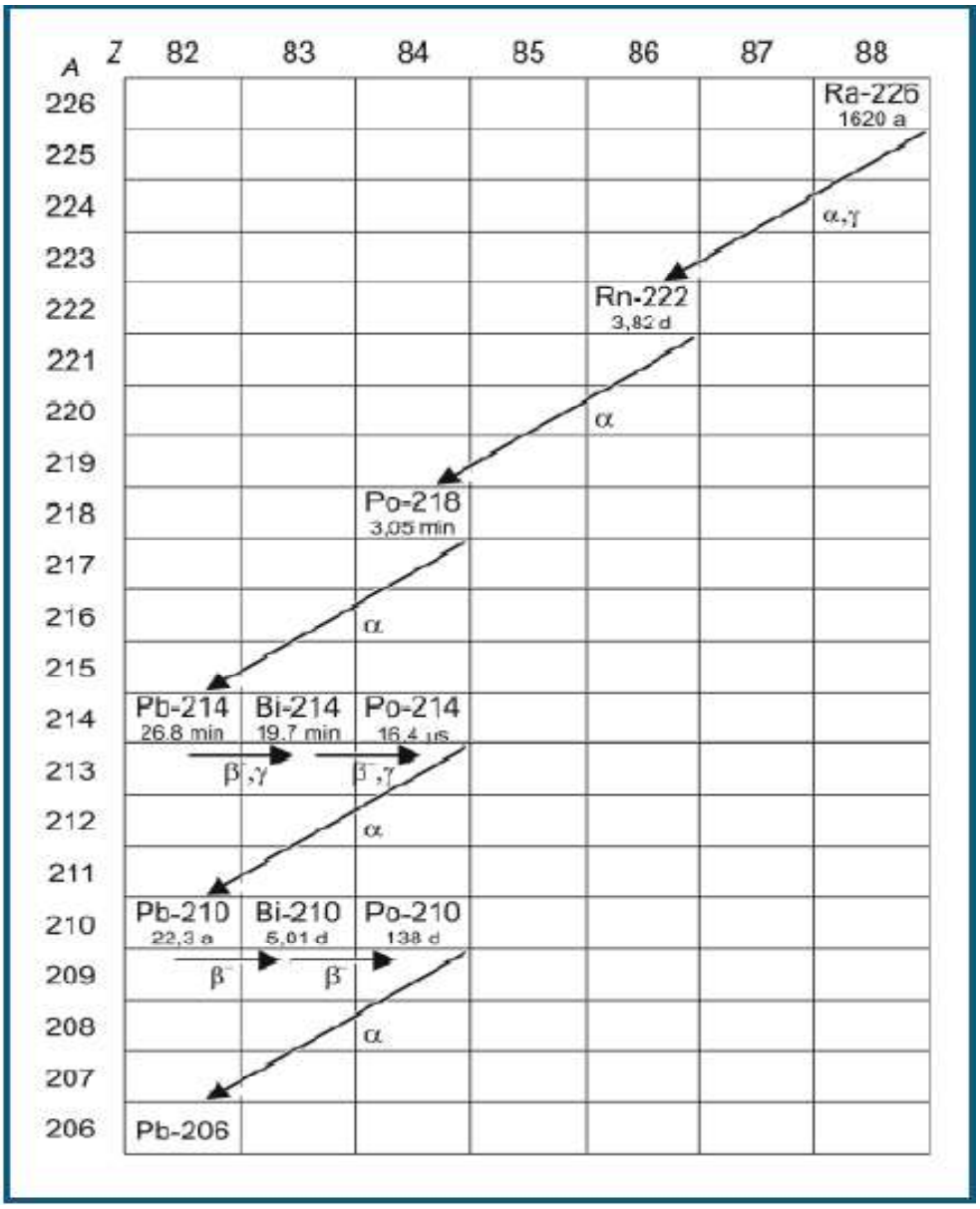

Figure 7 Decay series of uranium with its daughter nuclide

The mass number of isotopes in the uranium decay series can be represented as 4n+2. This decay series starts with the unstable radioactive ^{238}U and ends with the stable isotope ^{206}Pb. Figure 7 above shows the release of alpha- and beta-particles. The half-life of ^{238}U is recorded as 4.5 billion years. It should be noted that gamma-photons are also released at different energy levels by some isotopes. At the energy

level of 186keV ^{226}R a releases gamma-photons when decaying to ^{222}Rn. This is followed by ^{214}Pb decaying to ^{214}Bi at 352.295 keV, 242 keV and 53 keV. Gamma-photons are also released when ^{214}Bi decays to ^{214}Po at 609 keV. These are shown in Table 8.

^{238}*U Ingrowth*

^{238}U daughter nuclides grow in two groups. In the first group ^{234}Th has the longest half-life of the group. The group will take about 8 x $T_{1/2}$ of ^{234}Th to grow in and reach near equilibrium (Van Rooyen, 2012). The second group is the one where ^{234}U has the longest half-life. It will take about 8 x 2,5 million years to grow in and reach near equilibrium. At this stage of near full equilibrium the photon yield is 3.457. Different daughter nuclides have yields at different energies. These photon lines are unique to ^{234}U.

Table 8 Shows Energy and Yield lines that are indicative of the presence of ^{238}U in a sample (Van Rooyen, 2012)

^{238}U	
Photon Energy. MeV	Photon Emission Yield
0.60931	0.47068
0.35193	0.38389
0.29522	0.19705
1.76449	0.15723
1.12029	0.15417
0.07741	0.11261
0.01084	0.10325
0.24200	0.07586
0.07506	0.06735
0.01084	0.05932
1.23811	0.05912
2.20421	0.05187

0.76836	0.05044
0.06329	0.04834
0.00246	0.04750
0.04654	0.04339
0.01628	0.04180
1.37767	0.04084

Contribution of photons where ^{238}U is at equilibrium with its daughter nuclides comes mainly from ^{214}Pb (16.46%) and ^{214}Bi (80%). See Table 9 below

Table 9: Showing the contribution of the individual daughter nuclide in the ^{238}U decay series to the effective dose rate around an unshielded point-like source of ^{238}U at equilibrium with its daughter nuclide (Van Rooyen, 2012)

Nuclide	% Contribution to Photon DR
^{238}U	0.161
^{234T}h	0.8188
234Pa-m	0.9223
^{234}Pa	0.1294
^{234}U	0.2237
^{230}Th	0.1815
^{226}Ra	0.484
^{222}Rn	0.0246
^{218}Po	0.0541
^{214}Pb	16.461
^{214}Bi	79.962
^{214}Po	0.004969
^{210}Pb	0.5401
^{210}Bi	0.00002
^{210}Ti	0.032
^{210}Po	0.0006

2.4.4 Radiation laws

The rate at which radioactive material disintegrates, is referred to as activity, A. It is the number of disintegrations per unit time, t, and is denoted as follows:

$$A(t) = \lambda N(t) \quad (16)$$

Where:

$A(t)$ is activity at time t

$N(t)$ is number of disintegrations at time t

λ is decay constant

Looking at the time interval dt, which is from time t to $t + dt$, the decrease in the number of decaying nuclei is given by:

$$-dN(t) = \lambda N(t)dt \quad (17)$$

This implies that:

$$\frac{dN(t)}{N(t)} = -\lambda dt \quad (18)$$

By integrating both sides

$$N(t) = N_0 e^{-\lambda t} \quad (19)$$

Where

N_0 is number of disintegrations at time t_0

By multiplying both sides of equation 19 with λ gives

$$\lambda N(t) = \lambda N_0 e^{-\lambda t} \quad (20)$$

From equation 16

$$A(t) = \lambda N(t) = -\lambda N_0 e^{-\lambda t} \quad (21)$$

Therefore:

$$A(t) = \lambda N(t) = -A_0 e^{-\lambda t} \quad (22)$$

Where

A_0 is activity at time t_0

The activity decreases exponentially with time. The time where the activity has decreased to half of the original value is called the half-life, T1/2. See Figure 8 for illustration.

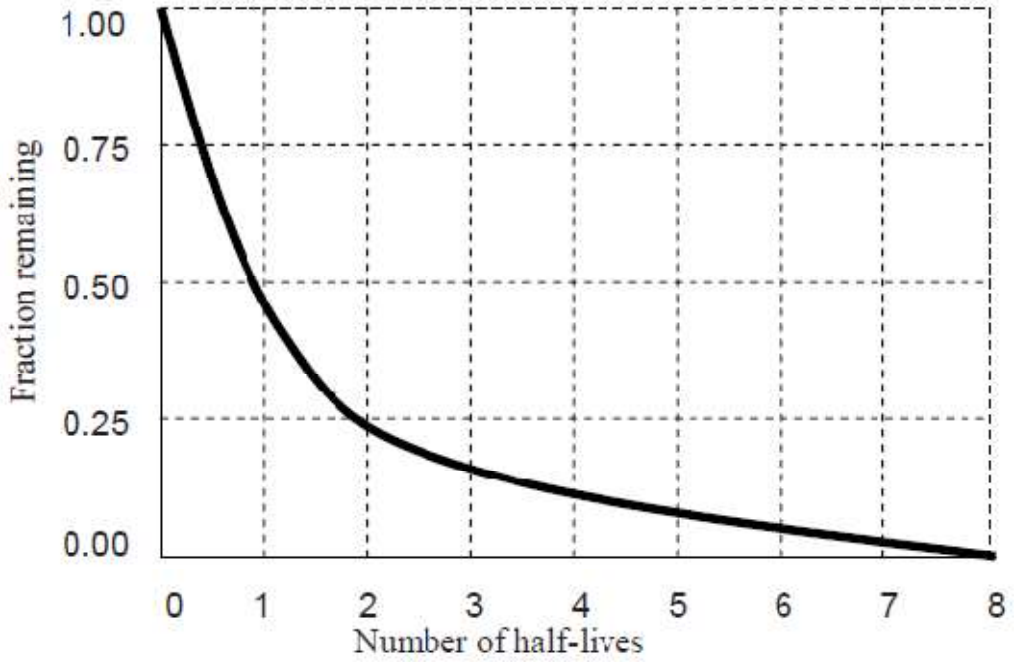

Figure 8 Proportion of initial nuclei remaining at time t (Jevremovic, 2009)

$$A(T_{1/2}) = \frac{A_0}{2} \tag{23}$$

Therefore from equation 22;

$$\frac{A_0}{2} = -A_0 e^{-\lambda T_{1/2}} \tag{24}$$

$$T_{1/2} = \frac{ln2}{\lambda} = \frac{0.693}{\lambda} \tag{25}$$

Therefore

$$\lambda = \frac{0.693}{T_{1/2}} \tag{26}$$

λ is inversely proportional to $T_{1/2}$

2.4.5 Bateman Equation

Daughter nuclides formed from parent nuclides also undergo radioactive decay to form their own daughter nuclides.

Equation 17 can be written as

$$\frac{dN_d}{dt} = -\lambda N_p \qquad (27)$$

The rate of change of daughter nuclide will then be denoted as:

$$\frac{dN_d}{dt} = \lambda_p N_p - \lambda_d N_d \qquad (28)$$

By substituting equation 20 into equation 28 gives:

$$\frac{dN_d}{dt} = \lambda_p N_{p0} e^{-\lambda_p t} - \lambda_d N_d \qquad (29)$$

Integration of both sides of equation 29 gives:

$$N_d = N_{d0} e^{-\lambda_d t} + \frac{N_{p0}\lambda_P}{\lambda_d - \lambda_p}\left(e^{-\lambda_p t} - e^{-\lambda_d t}\right) \qquad (30)$$

Equation 30 is written in terms of activity as:

$$A_d = A_{d0} e^{-\lambda_d t} + \frac{A_{p0}\lambda_d}{\lambda_d - \lambda_p}\left(e^{-\lambda_p t} - e^{-\lambda_d t}\right) \qquad (31)$$

At time t_0, $N_{d0} = 0 \; and \; A_{d0} = 0$

Therefore:

$$N_d = \frac{N_{p0}\lambda_P}{\lambda_d - \lambda_p}\left(e^{-\lambda_p t} - e^{-\lambda_d t}\right) \qquad (32)$$

And

$$A_d = \frac{A_{p0}\lambda_d}{\lambda_d - \lambda_p}\left(e^{-\lambda_p t} - e^{-\lambda_d t}\right) \qquad (33)$$

The n^{th} daughter radionuclide is represented as (Van Rooyen, 2012)

$$N_n(t) = N_0 \left(\prod_{p=1}^{n-1} \lambda_p \right) \sum_{j=1}^{n} \left(\frac{e^{-\lambda_j t}}{\left(= 1 \; if \; \lambda_p - \lambda_j = 0 \right) \prod_{p=1}^{n} \left(= \lambda_p - \lambda_j \; otherwise \right)} \right) \quad (34)$$

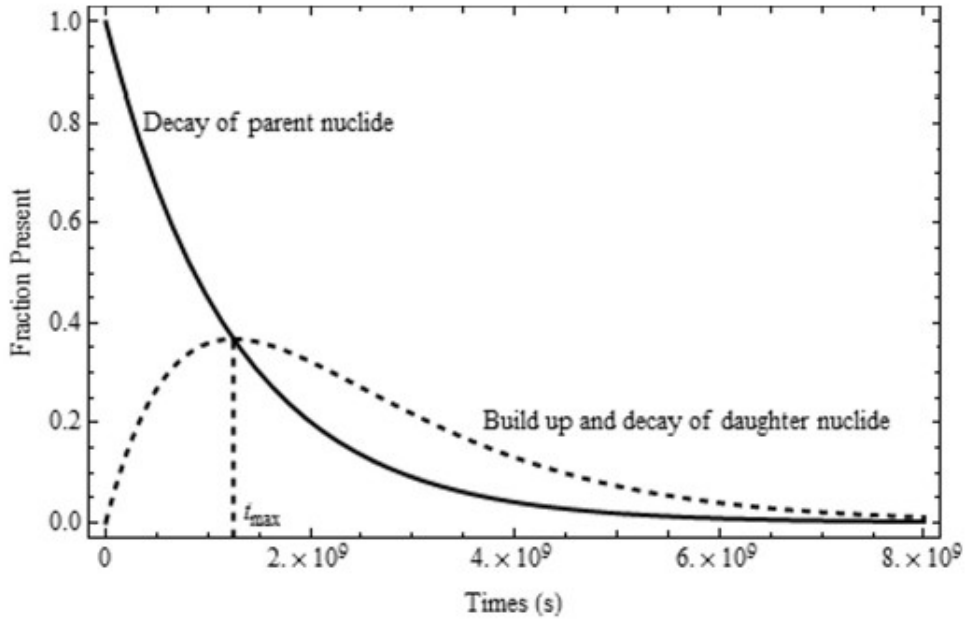

Figure 9 General trend of activity change with time (Jevremovic, 2009)

The time,t_{max}, for the daughter nuclide to reach its maximum activity is obtained by differentiating equation 32 to give:

$$\frac{dN}{dt} = \frac{d}{dt}\left[\frac{N_{p0}\lambda_P}{\lambda_d - \lambda_p} \left(e^{-\lambda_p t} - e^{-\lambda_d t} \right) \right] = 0 \quad (35)$$

This is depicted on Figure 9. This implies that:

$$\frac{N_{p0}\lambda_P}{\lambda_d - \lambda_p} \left(-\lambda_p e^{-\lambda_p t_{max}} - \lambda_d e^{-\lambda_d t_{max}} \right) = 0 \quad (36)$$

$$\lambda_p e^{-\lambda_p t_{max}} = \lambda_d e^{-\lambda_d t_{max}} \quad (37)$$

$$t_{max} = \frac{ln\left(\frac{\lambda_d}{\lambda_P}\right)}{\lambda_d - \lambda_p} \quad (38)$$

Therefore the maximum time for the daughter nuclide to reach its maximum activity depends only on its decay constant and the parent nuclide decay constant.

2.4.6 Decay Equilibrium

When analysing environmental samples it is important to confirm if the sample has reached equilibrium. There are three types of equilibrium for radioactive material.

2.4.6.1 Secular Equilibrium

Secular equilibrium can only be obtained when the half-life of the parent radionuclide corresponding to the decay constant λ_p, is much greater than the half-life of the daughter radionuclide corresponding to decay constant λ_d.

From equation 25, an increase of half-life means a decrease in λ. This means Secular Equilibrium is achieved when $\lambda_d > \lambda_p$

From the equation 33, assuming that daughter activity is 0 initially,

$$A_d = \frac{A_{p0}\lambda_d}{\lambda_d - \lambda_p}\left(e^{-\lambda_p t} - e^{-\lambda_d t}\right) \quad (39)$$

For $\lambda_d > \lambda_p$ it implies that

$$A_d = \frac{A_{p0}\lambda_d}{\lambda_d}\left(e^{-\lambda_p t}\right) = A_{p0}\left(e^{-\lambda_p t}\right) = A_p \quad (40)$$

This shows that Secular Equilibrium is achieved when the activity of the parent radionuclide is equal to the activity of the daughter radionuclide. See Figure 10.

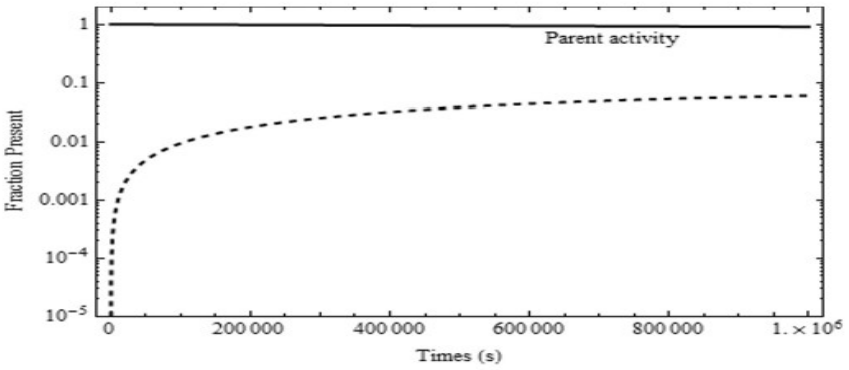

Figure 10 Daughter nuclei build-up and reaching near equilibrium with parent nuclei (Jevremovic, 2009)

2.4.6.2 Transient Equilibrium

Transient Equilibrium is achieved when the half-life of the parent radionuclide corresponding to the transition constant λ_1, is not much greater than the half-life of the daughter radionuclide corresponding to constant λ_2.

That is,

$$\lambda_d > \lambda_p$$

From the equation 33

$$A_d = \frac{A_{p0}\lambda_d}{\lambda_d - \lambda_p}\left(e^{-\lambda_p t} - e^{-\lambda_d t}\right) \qquad (41)$$

It implies that

$$A_d = \frac{A_{p0}\lambda_d}{\lambda_d - \lambda_p}\left(e^{-\lambda_p t}\right) \qquad (42)$$

Therefore the activity of the daughter radionuclide overshoots that of the parent as shown on Figure 11 and gradually decreases at nearly the same rate as that of the parent. In this case Transient Equilibrium is achieved.

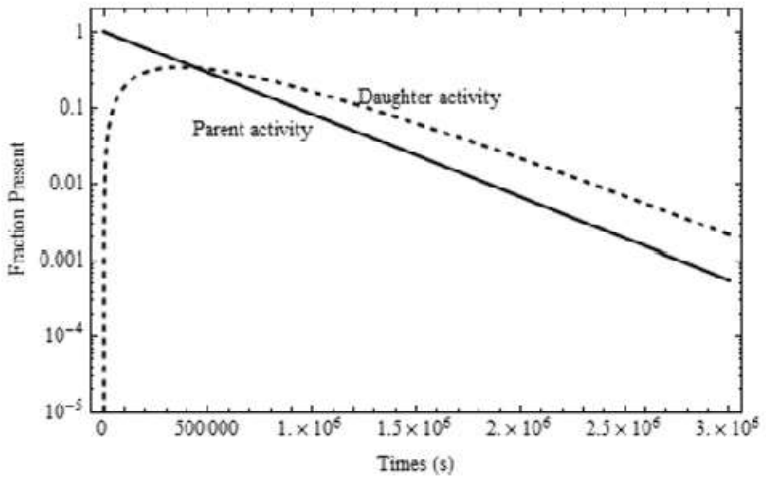

Figure 11 Daughter nuclei build-up overshoot and decay at same rate as parent nuclei (Jevremovic, 2009)

2.4.6.3 No Equilibrium

No Equilibrium is achieved when the half-life of the parent radionuclide corresponding to the decay constant λ_p, is less than the half-life of the daughter radionuclide corresponding to decay constant, λ_d

That is,

$$\lambda_d < \lambda_p$$

From equation 33

$$A_d = \frac{A_{p0}\lambda_d}{\lambda_d - \lambda_p}\left(-e^{-\lambda_d t}\right) \qquad (43)$$

The total activity is mainly due to the daughter activity. The daughter nuclide builds up faster than it decays until the parent nuclide has completely decayed. There will be no equilibrium reached with the parent radionuclide.

2.5 Exposure pathways to NORM from natural gas pipelines

The NORM is harmless when left in their natural form and location. The oil and gas extraction and the operation and maintenance of the gas transmission pipelines

disturb this natural occurrence and concentrate the NORM to harmful levels. The following groups of people are exposed to health issues related to TERNORM (Thompson, 2015)

- Workers operating and doing maintenance on gas lines
- Inspectors of gas lines
- Workers at waste treatment facilities

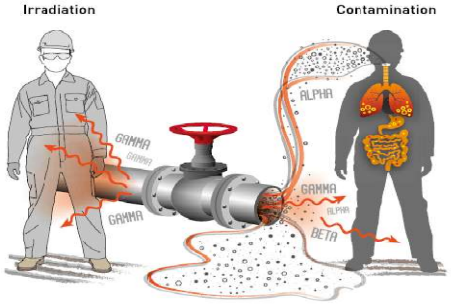

Figure 12 Exposure of workers to radiation in oil and gas industry (IOGP, 2016b)

Radioactive material can enter the body by inhalation, ingestion or absorption as shown on Figure 12. The health effects of ionizing radiation depend on amount of energy taken into the body, time, dose rate and body part exposed to radiation. It should also be noted that radiation may be low but concentration could be high.

2.6 Health effects of radiation and Dosimetry

2.6.1 Health effects

The health effects of Ionising Radiation are categorised as:

i. Deterministic which relates to tissue reactions
ii. Stochastic effects which relates to
    a. Risk of Radiation-related cancer, RRC
    b. Risk of Heritable ill health, HIH

Based on studies done on survivors of Hiroshima and Nagasaki bombings, Van Rooyen (2020), it has been established that ionising radiation is a carcinogen. However, ionising radiation is a manageable cancer risk factor. Hence it is necessary to analyse and characterise radioactive waste in work environment.

Workers who are exposed to radiation are at risk of RRC more than HIH. It has been shown using Excessive Relative Risk Values, Van Rooyen (2020), that RRC mortality

increases by about 29% per decade decrease in age at exposure. This means that it is more risky to continuously receive a dose at 25 years than at 35 years even if it is below dose limits and threshold. The study has also shown that risk of HIH in adult workers is 0.1% per 1Gy of gonadal radiation dose. Therefore, for workers, risk of RRC outweighs the risk of HIH at dose rates below exposure limits and thresholds. The organs more prone to RRC are breasts, ovaries, bladder, lungs, bone marrow, colon and stomach.

In most oil and gas facilities including the Komatipoort ROMPCO operation, extensive safety and health measures and procedures have been instituted to protect workers from Deterministic effects relating to tissue reactions. At ROMPCO in Komatipoort, safety officers measure radiation dose rates around the “pig” receiver before they are opened in order to remove dust that has been collected from the pipeline. It is mandatory for workers and safety officers to wear appropriate PPE and this is adhered to regularly.

2.6.2 Dosimetry

According to OHS Act 85 of 1993 Article 13(a): Duty to inform, it states that:
“*The employer must make every employee conversant with any health and safety hazards attached to work, production, processing, handling, storing, transporting and precautionary measures*.” Van Rooyen (2020)
It is therefore important for the employer and employees to know if there is a risk of ionising radiation in the work environment and hence the need for measurement and quantification. Ionising radiation is expressed as equivalent dose, H_T, in tissue or for the different parts of the body and as effective dose E for the whole body. In both cases it is expressed in the units of Sieverts (Sv). Let us define the following quantities:

2.6.2.1 Absorbed Dose

Absorbed dose is the amount of energy absorbed from radiation by a unit mass of tissue or body part. Absorbed dose from radiation R to tissue T is defined as

$$D_{T,R} = \frac{d\epsilon}{dm} \qquad (44)$$

Where:

$d\epsilon$: is mean energy from ionising radiation

dm: is mass of tissue or body part

The unit is gray (Gy) where $1\ Gy = 1\ J.kg^{-1}$

2.6.2.2 Equivalent Dose

Different types of radiation have diffrent impact on body tissue or organ. It is therefore necessary to have weighting factors for different types of radiation when looking at radiation protection. Equivalent dose is a quantity used to measure damaging absorbed dose by different types of radiaion on the same tissue or organ. It is mathematically defined as:

$$H_T = \sum_R w_R D_{T,R} \tag{45}$$

Where:

w_R : is radiation weighting factor for ionising radiation R

H_T : Average equivalent dose in organ or tissue T

2.6.2.3 Effective Dose

In the case where more than on tissue or body organ is exposed to more than one type of radiation, an effective dose, E, is calculated. Owing to the fact that different tissues will be damaged differently, a tissue weighting factor w_T is introduced such that

$$E = \sum_T w_T \sum_R w_R D_{T,R} \tag{46}$$

2.7 Radiation measurement and detection

2.7.1 Interaction of gamma photons with matter

The interaction of photons with matter and hence attenuation of these photons depends on (i) atomic number of the elements in the matter, (ii) density of the matter and (iii) energy of ionising photons as shown by Figure 15. Photons interact with matter in the following manner:

2.7.1.1 Photo-electric absorption

The photon is completely absorbed in the material that it interacts with. The absorbed energy is imparted to the bounded electrons. When the imparted energy is greater than the energy binding the electron to the atom then the electron will be released. The most probable electrons to be released are the K-shell electrons. This is illustrated on Figure 13.

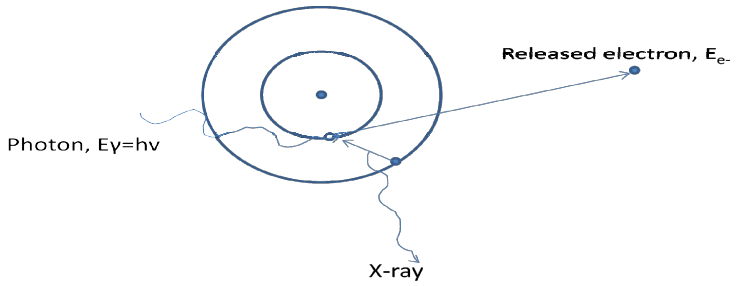

Figure 13 Ionisation of an atom (Ahmed, 2007)

The emitted electron is called a photo-electron. The photo-electron leaves a vacancy in the K-shell. This vacancy is filled by one of the electrons in the outer shells. When this electron drops down to fill the vacancy it releases energy in the form of X-rays.

2.7.1.2 Compton scattering

Compton scattering is an elastic collision between an incoming photon and an electron in the atom of the material. The incident ionising photon is not completely absorbed but is deflected at an angle by the electrons in the atoms of the material. A recoil electron is then released. This type of collision is illustrated on Figure 14.

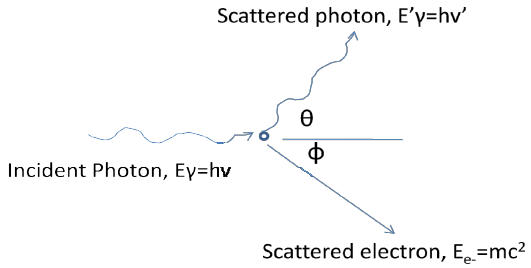

Figure 14 An elastic Compton scattering (Santawamaitre, 2012)

Energy of scattered photon is given in terms of incident photon by (Santawamaitre, 2012)

$$E'_{\gamma} = h\upsilon' = \frac{h\upsilon}{\left(1 + \left(\frac{h\upsilon}{m_o c^2}\right)(1 - \cos\theta)\right)} \qquad (47)$$

The interaction is with weakly bonded electrons to the atom. The microscopic cross-section, σ, is dependent on the number of electrons in the atom such that

$\sigma_{cs} \propto Z$

But

$\mu = N\sigma$

and

$N \propto \frac{\rho}{Z}$

Therefore

$\mu_{cs} \propto \left(\frac{\rho}{Z}\right) Z$

$\mu_{cs} \propto \rho$

The above relations show that in Compton scattering the macroscopic cross-section dependent on the density of the material.

2.7.1.3 Pair production

In the case of pair production the interaction of the photon with matter results in the release of an electron and positron pair.

$$\gamma + X \rightarrow e^- + e^+ + X^*$$

For this to happen the incident gamma-photon must have energy greater than twice the rest-mass energy of an electron (Ahmed, 2007)

$$E_\gamma > 2m_e\,c^2 = 2 \times 0.511\,MeV = 1.022\,MeV \quad (48)$$

The excess energy after the creation of the electron-positron pair is imparted to the electron and positron as kinetic energy such that

$$E_{e^-} + E_{e^+} = E_\gamma - 2m_e\,c^2 \quad (49)$$

Based on the law of conservation of energy and momentum third particle is needed to act as a recoil particle. Therefore the threshold energy required for pair production is

$$E_{pp,threshold} = 2m_e\,c^2\left(1 + \frac{m_e}{M}\right) \quad (50)$$

M is the mass of the recoil particle

The electron-positron pair will interact with other charged particles in the matter. This interaction will lead to the loss of energy through ionisation, excitation and/or Bremsstrahlung process. Owing to the high energy required for this interaction, pair production dominates where energy of incident gamma-photons is greater than 5MeV. In this region the microscopic cross-section of pair-production, σ_{pp}, is directly proportional to the square of the atomic number

$$\sigma_{pp} \propto Z^2$$

The macroscopic cross-section is directly proportional to the product of density of the matter and atomic number

$$\mu_{pp} \propto \rho Z$$

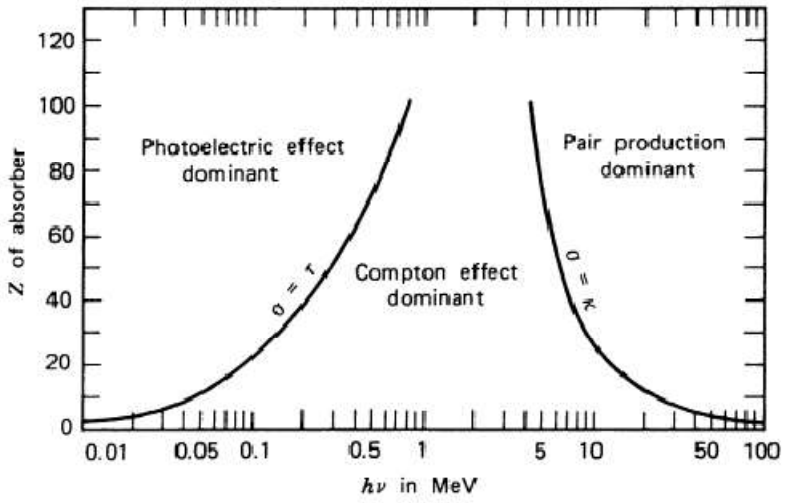

Figure 15 Different types of ionising radiation interaction with matter (Santawamaitre, 2012)

2.7.2 Types of radiation detectors

In this section a brief discussion of 3 types of radiation detectors is given.

2.7.2.1 Gas filled detectors

In section 2.7.1 it was pointed out that when photons goes through material, in this case gas, the photons will either be completely absorbed or partially absorbed. If they have enough energy they will dislodge ion pairs from the atom and thus ionizing the gas molecules. An electric field is applied to the produced electron pair and the pair of charged particles will move into opposite directions. The movement of these charged particles create an electric pulse which can be measured. A typical gas-filled detector consists of gas chamber/enclosure, an anode and a cathode forming parallel plates, a resistor and a voltage supplier as shown on Figure 16.

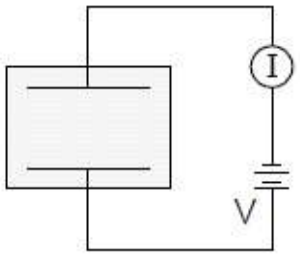

Figure 16 A simplified schematic of gas-filled detector (MacMaster)

There are several regions of operation for gas-filled detectors. They are determined by the voltage applied on the electron pairs (Ahmed, 2007). When there is no electric field applied the electron pair will recombine. This is the recombination region. It is fruitless to operate the detector in this region because the absorbed energy will not be correctly reflected. A gradual increase of the applied voltage will ensure that the electrons do not recombine.

At a point where the voltage applied is enough to prevent recombination of the electron pairs, that is the beginning of the ionisation chamber region. In this region ionization is higher for α-particles than for β-particles. In this region an α-particles produces a pulse larger than a β-particles by an order of 10^3. Increasing the applied voltage will accelerate the produced electron pair. At high velocities these electron pairs contain high enough energy to start secondary ionization. If the resultant electron pairs from the initial ionisation have enough energy they will initiate further ionization. The number of secondary electrons produced is proportional to the number of initial electrons produced. The output pulse is stronger from all these multiplied electrons and is proportional to the amount of energy initially deposited. This is the proportional counter region. In this region both α-particles and β-particles produce higher pulse heights but the α-particles are even better. The applied voltage varies between 2 and 4keV (Lieser, 1997). Further increase of the applied voltage leads to an avalanche of electron pairs. The absorption of electrons at the anode leads to release of photons. The photons in turn results with the emission of photo-electrons. This region at this energy level is called the Geiger-Mueller region. The avalanches trigger a release of more positive ions which deposit at the anode and cover the anode. At this stage no counting takes place and there is a dead-time caused by the layer of positive ions. A quench gas is normally inserted to minimise the negative effects of positive ions. There is no correlation between the pulse height and the energy deposited by the incident photons. This means that they cannot be utilised to discriminate between types of radiation and their energies.

2.7.2.1.1 Scintillation detectors

There are two types of organic scintillators associated with scintillation detectors, namely, organic and inorganic scintillators. In the case of organic scintillators the incident photons deposit their energy into the molecule and excite the electrons into a number of excited states, S-states S1, S2, S3… S10, S11, S12 (MacMaster). All other states except S10 de-excite and loose energy quickly. So immediately after the incident photon strikes the organic scintillator there will be molecules in excited state S10. Light photons are emitted when these molecules go back to ground state. However, in the case of inorganic scintillators, it is the structure of the crystal lattice of the scintillator that plays a crucial role. Incident photon with high energy excites an electron deep in the valence band. This excited electron jumps through the energy gap into the conduction band and leaves behind a positive hole. An electron with higher energy in the valance band fill the hole and in so doing emits light photons.

In both cases of organic and inorganic scintillation the light photons are then guided to the photo cathode in the photon multiplier tube, PMT. The light photon deposits energy into the photo-cathode and photo-electrons are emitted. These photo-electrons are multiplied, subjected to an electric field to give a pulse that can be analysed. The schematic is shown on Figure 17.

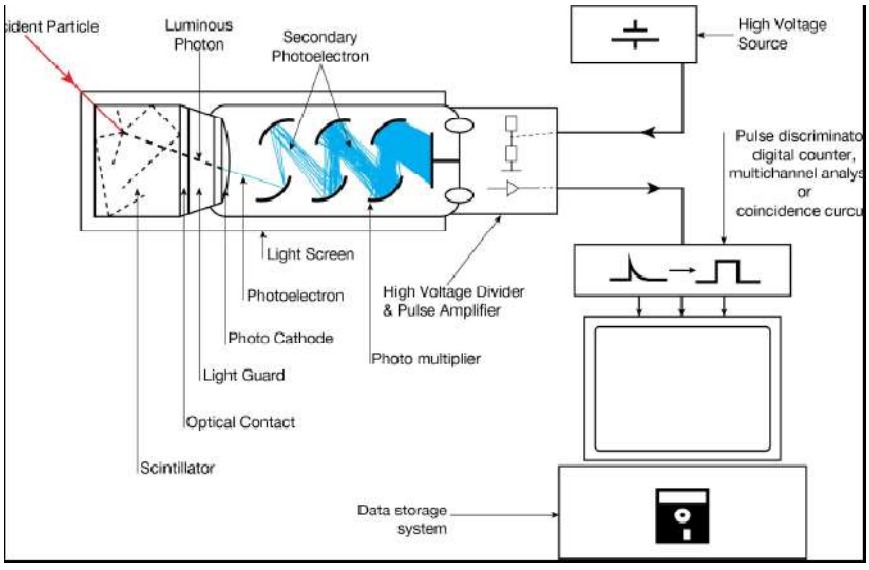

Figure 17 A schematic of a scintillation detector (online picture)

The advantages of scintillation detectors are;

- Efficiency
- High precision and counting rates
- The amplitude of the pulse is proportional to the energy of the incident photon

2.7.2.1.2 Solid state detectors

Similar to inorganic scintillators, the structure of the crystal lattice of the material that absorbs the photon energy is crucial. Covalent bonding between atoms in the solid material creates discrete energy levels (Ahmed, 2007). These energy levels are grouped into two energy bands, namely, the valence band and the conduction band as shown on Figure 18. The energy levels of the valence band are closely spaced and are of low energy. The energy levels of conduction band are high. There is a gap between these two energy bands called the band gap or energy gap. In the valence band electrons are bonded strongly to their atoms whereas electrons in the conduction band move freely. The electrons in these energy bands give the solid material its electrical conducting properties. The solid material could be an insulator, semi-conductor or a conductor of electricity. The energy gap for an insulator is >5eV and for the semi-conductor it is <2eV (Santawamaitre, 2012)

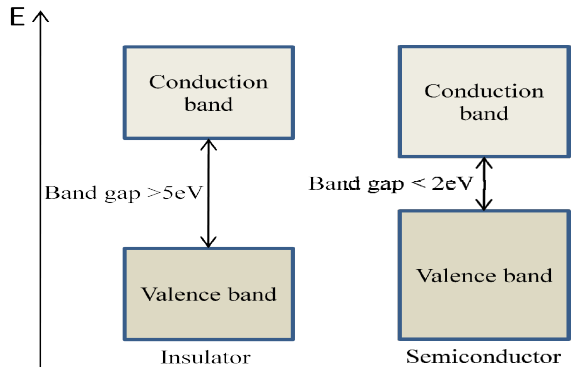

Figure 18 Energy bands in a detector material (Ahmed, 2007)

An incident photon with high energy excites an electron deep in the valence band. This energised electron jumps through the energy gap into the conduction band and leaves behind a positive hole. These electron-hole pairs change the conductivity of the semiconductor. When an electric field is applied to these charge carriers they

move to the opposite direction creating a change in electric current. The change in conductivity and hence the change in electrical current is proportional to the energy of the incident photon.

In the case of a semiconductor the electron may jump through the energy gap due to a rise in temperature or thermal energy. The probability of this happening is given by (Santawamaitre, 2012).

$$p(T) = CT^{3/2} exp\left(-\frac{E_g}{2kT}\right) \quad (51)$$

Where T = absolute temperature

E_g is band gap energy

k is Boltzman constant

C is Proportionality constant

Impurities in small amounts can be added into the material of the semi-conductor. This phenomenon is called doping. The impurity is an element with different outer atomic shell to that of the semi-conductor. This adds additional energy levels between the valence band and the conduction band. Depending on the type of element added these energy levels could be located near the valence band with more positive charges. These are called the acceptor impurity. The impurity could add more energy levels towards the conduction band creating more negative charges. These are called the donor impurity. A semiconductor with acceptor impurity is called p-type and the one with donor impurity is called n-type. The acceptor and donor energy levels in a detector are illustrated on Figure 19.

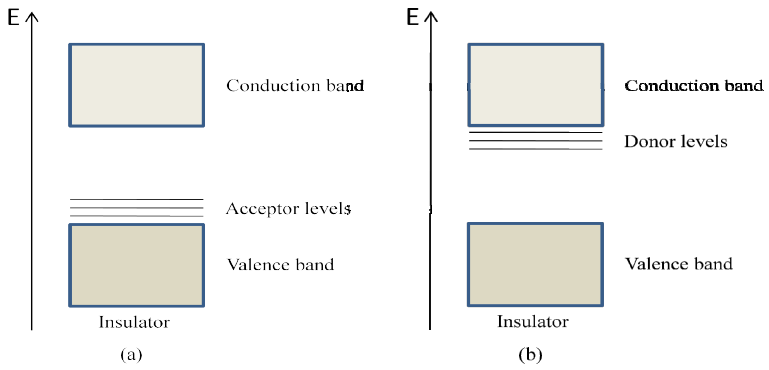

Figure 19 Acceptor and donor energy levels in a detector material (Ahmed, 2007)

2.7.2.1.3 Choice of detectors

The choice of a detector depends on the following: (Lieser, 1997)

a. The type of sample; gas, liquid or solid
b. The type of ionising radiation particles being analysed
c. The energy level of the ionising radiation particles being analysed
d. Requirement for efficiency or resolution

Gas samples must be analysed with gas ionisation chambers, proportional counters and Geiger-Mueller counters. Choosing one of these three detectors will depend on the energy level of the ionising radiation particles being analysed. Table 10. Liquid samples must be analysed with liquid scintillation detectors. However, for samples emitting high energy β-particles and γ-particles Geiger-Mueller counters can be used. For solid samples proportional counters must be used for α-particles and β-particles, and Geiger-Mueller counters must be used for high energy β-particles. Solid samples emitting γ-particles must be analysed with scintillation detectors and semiconductor detectors. Scintillation detectors must be used where efficiency is required and semiconductors must be used where resolution is of outmost importance.

Table 10 Suitability of detectors for the measurement of radiation (Lieser, 1997)

Kind of Radiation	Ionisation chamber	Proportional counters	Geiger-Mueller counters	Scintillation detectors	Semiconductor detectors
α radiation	Favourable	Favourable	Unfavourable	Liquid Scint. Favourable	Si barrier detectors favourable
β radiation (>1 MeV)	Unsuitable	Suitable	Favourable	Org. crystal favourable	Si barrier detectors suitable
β radiation (<0.5 MeV)	Unsuitable	Favourable	Unfavourable	Liquid Scint very favourable	Si barrier detectors favourable
γ radiation	Unsuitable	Unsuitable	Unfavourable	NaI(Tl) cryst. very favourable	Ge(Li) cryst. very favourable

2.7.2.1.4 High purity germanium, HPGe, detector

The high purity germanium detector is a semi-conductor detector. It is made-up of an intrinsic region which is sensitive to ionising radiation such as photons. The intrinsic layer is made up of atoms from group IV and in the case of HPGe it is a germanium crystal. Either side of the intrinsic region is coated with a p- or n-electrode (Mirion, 2020a). This is also called doping. As discussed in section 2.7.2.1.2 the 4 electrons in the outer shell form covalent bonds. The 5th electron of atoms in group V are weakly bonded and can easily be given away. Doping with atoms from this group such as phosphorus creates a donor layer that is negatively charged. Atoms from group III have an open valence bond. Doping with these atoms such as boron create a positively charged holes in the layer (Eckstein, 2012).

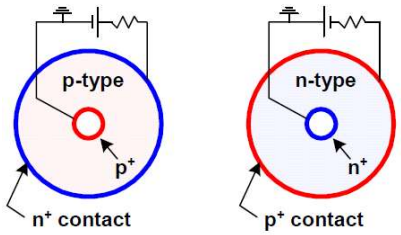

Figure 20 Electrode configuration for coaxial detectors (MacMaster)

A high voltage bias is applied across the electrodes until the crystal is depleted. When n^+ contact is on the outer surface the coaxial detector is called p-type and when it is in the inside it is called n-type. When a gamma ray strikes the depleted region the photon energy is absorbed and an electron hole charge carrier pair is formed. The charges are then swept to the p and n electrodes by voltage application as shown by Figure 20 and 21 for a coaxial detector. This will be converted to an electric pulse by the preamplifier(Mirion, 2020a).

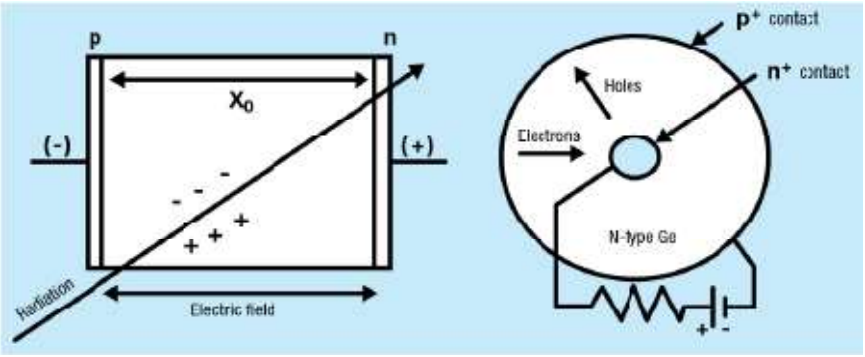

Figure 21 Showing a typical p-i-n junction with reverse bias and a cross section of an n-type detector (Mirion, 2020a)

Energy resolution of HPGe is given by

$$FWHM = \sqrt{(w_d^2 + w_c^2)} \quad (52)$$

Where

w_d is peak width due to detector effects

w_e is the peak width due to electronics effects

The following equation can be used to calculate w_d

$$w_d = 2\sqrt{(2ln2)F * E(keV) * w} \quad (53)$$

In equation 53 F is the fano factor and w is the energy required to produce an electron-hole pair charge carrier. In the case of HPGe w is approximately 3eV. The width w_e depends on the size of the detector and bias voltage. In order to improve energy resolution FWHM must be minimal. This can be achieved by minimizing detector size and bias voltage but not compromising on the benefits of higher bias voltage and larger detector.

In section 7.2.1.3 it was highlighted that at high energy levels the interaction of photons with matter will follow the pair production mechanism and the Compton scattering will be at low energies. This is what happens in the case of HPGe. Although the majority of photons absorbed are at higher energies, the Compton

scattering effect will still be observed at low energies. Most HPGe detectors are equiped with capabilities to minimize Compton scattering effect.

The different components of the HPGe spectrometric system are shown in Figure 22.

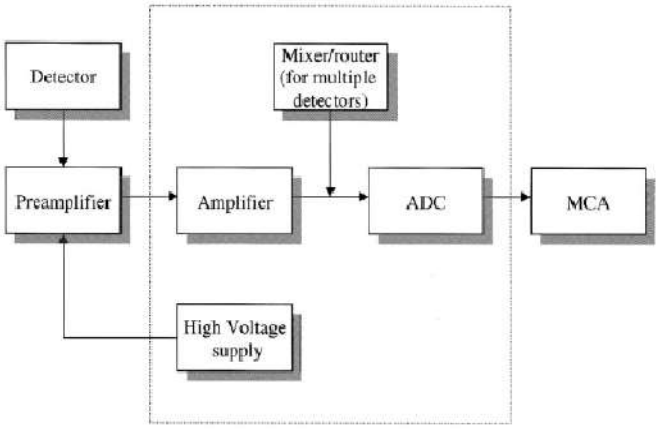

Figure 22 Components of gamma-spectrometric system (Wallbrink et al., 2002)

3 Methods

3.1 Study Area

The natural gas pipeline in this study is a 0,66 m ID pipeline running for about 860 km from Temane in the province of Inhambane in Mozambique to Secunda in the province of Mpumalanga in South Africa. There are five scraper stations along the pipeline numbered STS1 up to STS5. All the scraper stations can launch and receive a pig. The pipeline is buried underground and only surfaces when it reaches a scraper station. A compressor has been installed at STS4 in Komatipoort with dust filters on the inlet section. A scraping pig was launched in Temane in Mozambique and was received in Komatipoort at STS4 just before the compressor. The scale which had turned into dust coming from inside the pipeline was pushed out and received with the pig. This dust was collected into marked drums and stored in shipment containers.

Figure 23: Drums of waste from a pigging exercise stored in a shipment container

3.2 Sampling and sample preparation

Samples were taken from the stored drums as shown on Figure 23. There are 5 drums containing radioactive waste from pigging. Drums were numbered as they got filled. The first drum numbered #1 was filled first as scale arrived from pigging. The last drum was #5. Ideally all drums should have been sampled but the middle drums were not easily accessible or the samples would have required crushing and dying. Samples weighing about 1kg were collected into plastic sachets for transportation to be analysed.

When preparing samples for analysis it is important to consider geometry/shape, size and homogeneity of the material to be analysed. The samples collected are solid dry dust emanating from scale inside the gas pipeline. The sample does not need any chemical preparation or conditioning. However, the samples must be stored at room temperature. Holes were poked through the plastic sachets to make sure that they stay dry and do not get humid. A screen of 2mm apertures was used to screen the samples and ensure uniform size. See Figure 24 below.

Figure 24: Screening of samples using 2mm screens

Twenty screened samples coming from the first drum and twenty more samples from the fifth drum were collected into short transparent plastic bottles and sealed. Forty samples in total were prepared. The first 20 samples from drum #1 were labelled D1S1, D1S2, D1S3 … D1S20. The labelling is such that the D1 stands for drum #1 and S1 stands to sample 1 and so forth. Similarly with the second batch of samples it was labelled as D5S1, D5S2, D5S3, … D5S20. D5 stands for drum #5. Figure 25 shows labeled samples. After sealing the samples they were left for more than 30 days to ensure that equilibrium is reached between the parent radio nuclide and the daughter radio nuclide.

Figure 25 Labelled and sealed samples stored for more than 30 days to ensure equilibrium

3.3 Determination of natural radionuclides

3.3.1 Detector description

The analysis was carried out using the High Purity Germanium Spectroscopy, HPGe. The gamma ray spectrometer system is based on a high purity germanium (HPGe) coaxial well detector (GCW2021) with a total active volume of 142cc manufactured by Canberra industries. The HPGe detector will be cooled by liquid nitrogen from a vertical dipstick cryostat to reduce the reverse leakage current. The detector is housed in a cylindrical lead shield with a fixed bottom and a movable cover to reduce environmental background radiation so that the radionuclides activity from the soil samples at the natural level could be measured. The cylindrical shield of the detector is made from 10 cm thick low background lead and is internally lined with a 1 mm thick copper sheet to reduce the contribution from lead x-ray fluorescence. The detector system had a relative photopeak efficiency of greater than 20% and an energy resolution of less than 2.1 keV at the 1.33 MeV γ-photopeak of ^{60}Co. The associated electronics consisted of a built-in Canberra preamplifier model 2002CSL that is coupled with a Canberra multichannel analyser of the digital spectrum analyser (DSA-1000) for data acquisition. Display and analysis of the acquired spectra is performed by using a specialized computer program Windows based Genie 2000 software version 3.4 provided by Canberra industries. The detector system is shown on Figure 26.

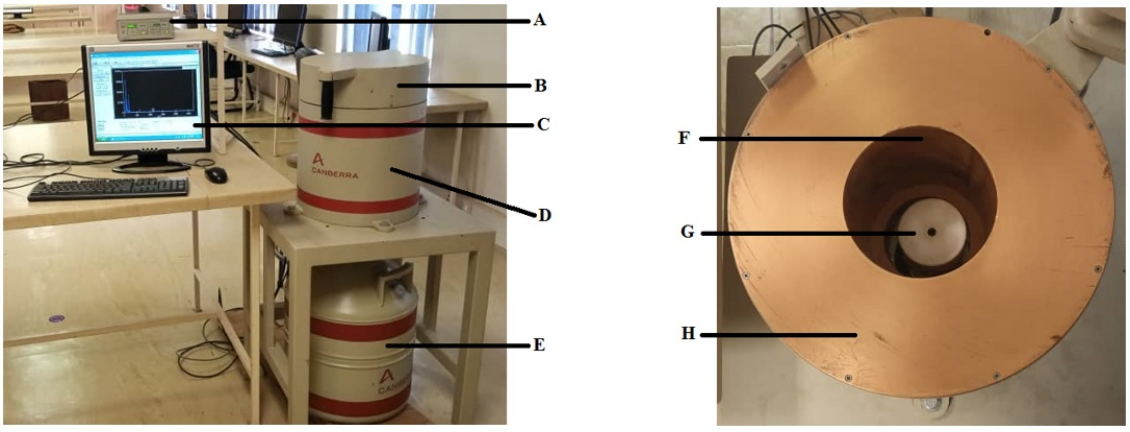

Figure 26: The HPGe detector system; (A) DSA-1000 multichannel analyser, (B) movable lead shield cover, (C) Computer for display and analysis of spectra (D) 10cm thick cylindrical lead shield, (E) liquid nitrogen dewar, (F) inner layer of 1mm

copper sheet, (G) well-type detector located at centre of lead shielding and (H) top layer of 1mm copper sheet.

3.3.2 Detector calibration

3.3.2.1 Energy calibration

The detector requires an energy calibration such that the energies match the corresponding channels. The channel-numbers on the MCA system are plotted against the gamma energies of specific radionuclides matching them with full energy peaks of the gamma rays. This is achieved by counting standard sources containing different radionuclides that will give energies over the range of interest (Wallbrink et al., 2002). It is ideal to use single gamma-ray emmitting radionucludes such as Ra-51 (320 keV), Cs-137(662 keV) and Mn-54(834 keV).

Multiple gamma-ray emmitting radionuclides can also be used but there will be coincidence summing effect.The excited states of the nucleus due to the absorbed photon last for picoseconds (Mirion, 2020b). However the interval between one detection and the next is in microseconds. Therefore the dtector will not differentiate between the multiple photon emmissions because the time between photon emmissions is shorter than the detector response time. The detector will give one single peak which is the sum of the two photon emmissions. This is called coincidence summing and is shown on Figure 27.

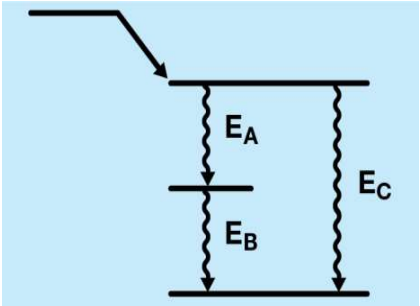

Figure 27**:** The multiple photon emmission demonstrating coincindence summing effect (Mirion, 2020b)

For the purpose of this investigation the RS_IAEA-RGU-1 reference for uranium was used and the RS_IAEA-RGTh-1 reference for thorium was used. A linear curve was produced by fitting a straight line in the different energy (keV) and channel coordinate points. The equation of the straight line is:

$$E = 0.04368 + 0.22 * channel\ number \quad (54)$$

The curve corresponding to this equation for the energy calibration is shown below in Figure 28.

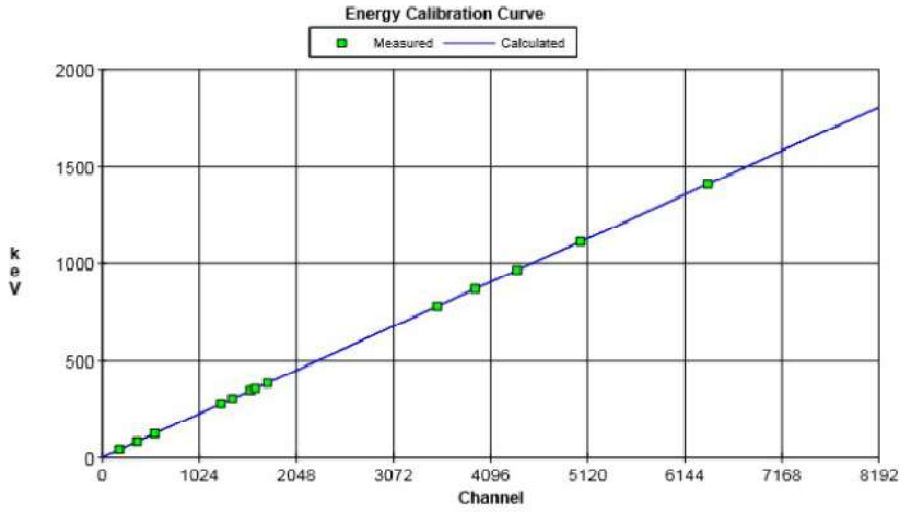

Figure 28: The energy calibration curve showing a plot of channel number against energy

3.3.2.2 Efficiency calibration

The photons emmitted by the source, sample, do not all reach the detector. Some are absorbed by the material between the detecor and the source and some leak. As a result it is important to know how efficient is the detector. Efficiency calibration is experimentally achieved by using a standard with known radionuclides and their activities. The specification sheet of the standard radionuclides will give the original activity and date when it was prepared. The photon emission intensity will also be given. There are two types of experimental efficiency. Full energy peak efficiency which is calculated using the peak net area and total efficiency which is calculated using the total area.

3.3.2.2.1 Full energy peak efficiency

The full energy peak efficiency, FEPE, as a function of energy for the detector is given by the following equation (Lépy, 2010)

$$\varepsilon_P(E) = \frac{N_P(E)}{AI_\gamma(E)} \quad (55)$$

Where $N_P(E)$ is peak net area at that particular energy, A is standard activity (Bq) and I_γ is photon intensity at that particular energy.

Different values of $\varepsilon_P(E)$ are calculated from experimental results at energies covering the range of interest. A curve can be fitted between two local energy and efficiency points. This is the interpolation method. The logarithmic curve is more accurate than a linear curve when the energy range is wide such as in this investigation. It is given by the following equation;

$$ln\big(\varepsilon_P(E)\big) = ln(\varepsilon_{P1}) + \frac{ln(E) - ln\,(E_{P1})}{ln(E_{P2}) - ln\,(E_{P1})} * (ln(\varepsilon_{P2}) - ln(\varepsilon_{P1})) \quad (56)$$

A mathematical function or polynomial may be fitted in a set of data with a wide range. The following mathematical relation is commonly used;

$$ln\big(\varepsilon_P(E)\big) = \sum_i^n a_i\,(lnE)^{-i} \quad (57)$$

Notes:

-The a_i coefficients can be determined using least-squares curve fitting

-Experimental data must be weighted

-The polynomial degree, n, must be far less than the number of experimental data.

When analyzing the data, dual curves were generated. One was at low energies and the other at higher energies. They were then spliced together to form one polynomial eqation given below:

$$ln\big(\varepsilon(E)\big) = -17.77 + 5.777 * ln(E) - 0.1517 * ln\,(E)^2 - 0.1443 * ln\,(E)^3 + 0.01231 * ln\,(E)^4 \quad (58)$$

This equation was derived from the efficiency curve below in Figure 29

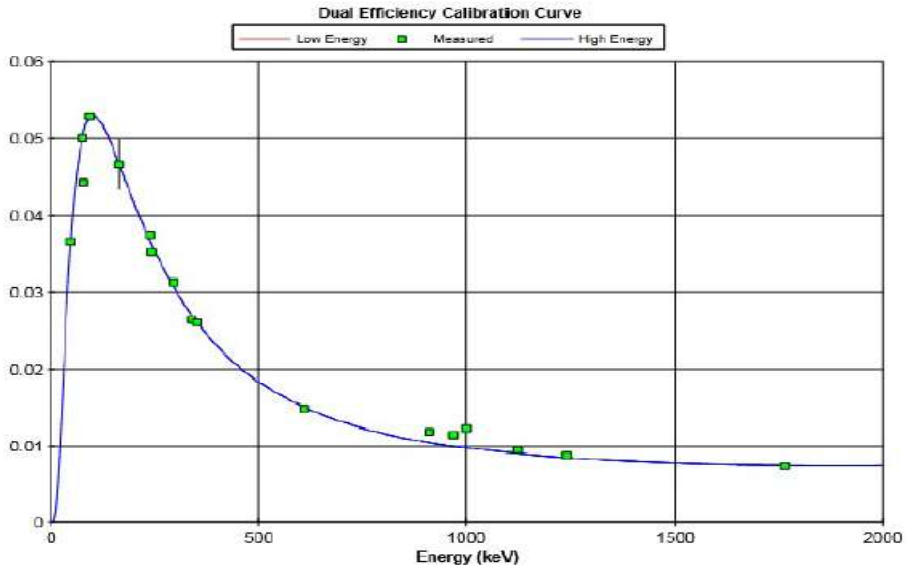

Figure 29: The efficiency calibration curve

3.3.3 Calculation of limiting levels and MDA in Genie by Mirion Technologies, Ref Persson (2019)

There are two main limiting levels as defined by Currie, Ref (Persson, 2019). They are:

L_C – Critical Level - The net signal level above which an observed signal may be reliably recognized as “detected”

L_D – Detection Limit – The “true” net signal level which may be a priori expected to lead to a detection

3.3.3.1 No signal detected

The variance of net signal is given by

$$\sigma_S^2 = (\sigma_{S+B}^2 + \sigma_B^2) = (S + B) + \sigma_B^2 \quad (59)$$

But at S=0 (no signal detected)

$$\sigma_0^2 = B + \sigma_B^2 \quad (60)$$

Expression for critical level is

$$L_c = k_\alpha \sigma_0 = k_\alpha \sqrt{B + \sigma_B^2} \quad (61)$$

For a 5% false positive rate, i.e, 95th percentile k = 1.645

This implies that

$$L_c = 1.645 \sqrt{B + \sigma_B^2} \quad (62)$$

For $B = \delta_B^2$ (approximation) and $S = 0$

$$L_c = 1.645\sqrt{2B} = 1.645\sqrt{2C} \quad (63)$$

Where

$$C\ is\ number\ of\ counts\ in\ continuum(number\ of\ counts\ in\ region\ of\ interest, ROI)$$

3.3.3.2 ROI of unidentified peaks

ROI is determined using FWHM at the energy of interest and it is assumed that the peaks follow a Gaussian distribution. Statistically it has been shown that

$$0.85FWHM = 1.985\sigma\ covers\ 95\%\ of expected\ counts$$
$$FWHM = 2.335\sigma\ covers\ 98\%\ of expected\ counts$$
$$1.25FWHM = 2.9195\sigma\ covers\ 99.6\%\ of expected\ counts$$

It should be noted that using a small region will lead to the exclusion of many counts which may give incorrect results. Figure 30 illustrates regions of interest.

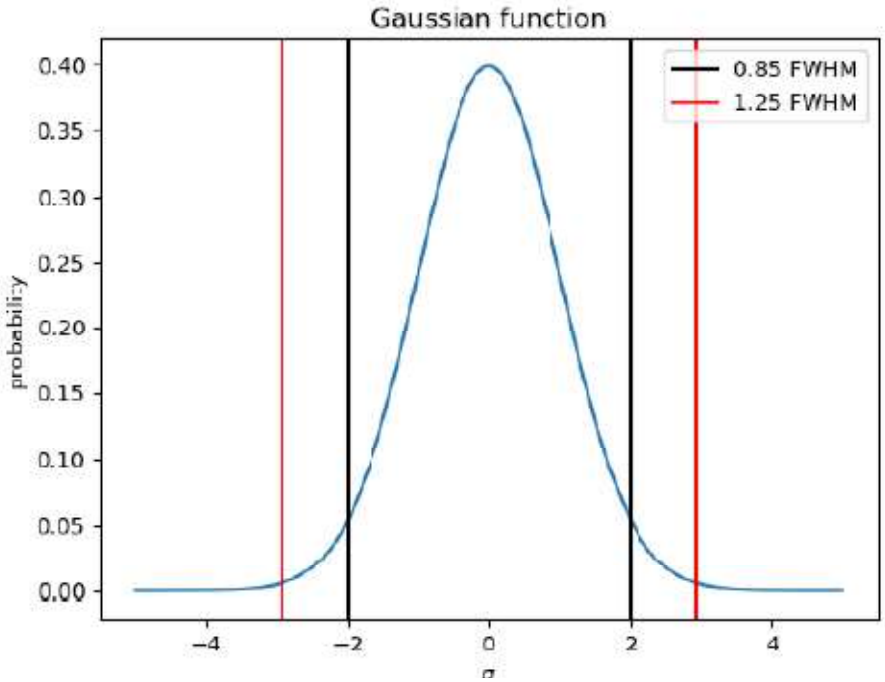

Figure 30: Illustration of regions of interest, ROI

3.3.3.3 Signal detected

For the case where a signal is detected the critical level is calculated as follows;

$$C = \left(\frac{N}{2n}\right)(B_1 + B_2) \tag{64}$$

And

$$\sigma_C^2 = \left(\frac{N}{2n}\right)^2 (B_1 + B_2) \tag{65}$$

Where

$B_1 and\ B_2\ are\ number\ of\ counts\ on\ either\ side\ of\ the\ region\ of\ interest, ROI$

$N\ is\ number\ of\ channels\ in\ the\ region\ of\ interest, ROI$

$n\ is\ number\ channels\ on\ either\ side\ of\ the\ region\ of\ interest, ROI$

$$L_c = 1.645\sqrt{C + \sigma_C^2} \tag{66}$$

$$L_c = 1.645\sqrt{\left(\left(\left(\frac{N}{2n}\right)+\left(\frac{N}{2n}\right)^2\right)(B_1+B_2)\right)} \quad (67)$$

The detection limit is calculated as follows;

$$L_D = L_C + k_\beta \sigma_D \quad (68)$$

But

$$\sigma_D^2 = L_D + \sigma_0^2 \quad (69)$$

This implies that

$$L_D = L_C + k_\beta\sqrt{(L_D + \sigma_0^2)} \quad (70)$$

From equation 61

$$\sigma_0 = \frac{L_C}{k_\alpha} \quad (71)$$

Substitute equation 71 in equation 70 and rearrange then;

$$L_D = L_C + \frac{k_\beta^2}{2}\left(1 + \sqrt{1 + \frac{4L_C}{k_\beta^2} + \frac{4L_C^2}{k_\alpha^2 k_\beta^2}}\right) \quad (72)$$

A common case occurs when

$$k = k_\alpha = k_\beta$$

Therefore;

$$L_D = k^2 + L_C = k^2 + 2k\sigma_0 \quad (73)$$

This approximates to;

$$L_D = 2.71 + 4.65\sqrt{C} \quad (74)$$

3.3.3.4 MDA calculation

The detection limit is calculated in counts. It is often desirable to convert to activity. This is done by applying a calibration factor which takes into account the detector parameters and response as follows:

$$MDA = \frac{L_D}{\varepsilon TIK} \tag{75}$$

By substituting equation 74 into equation 75

$$MDA = \frac{2.71 + 4.65\sqrt{C}}{\varepsilon TIK} \tag{76}$$

$\varepsilon\ is\ detector\ efficiency$

$T\ is\ counting\ time$

$I\ is\ Intensity$

$K\ is\ Conversion\ factor$

The MDA is given in Bq/kg and is inversely proportional to the counting time. Increasing the counting time decreases the MDA.

3.3.4 Counting and background counting

Each sample was left to count for 12 hours. There is background radiation everywhere which may interfere with sample radiation counting. This background radiation must be subtracted from results in order for the results to reflect sample radiation only. Background activity is subtracted from the total activity to get net activity efficiency as shown in the following relation; (Wallbrink et al., 2002)

$$\varepsilon = \left(\frac{\mathrm{C}_0}{\mathrm{T}_0} - \frac{\mathrm{C}_b}{\mathrm{T}_b}\right) * \frac{1}{M_0(\mathrm{A}_0 e^{-\lambda(t-\mathrm{t}_0)})} \tag{77}$$

Where

$C_0\ is\ Total\ count$

$T_0\ is\ Count\ Time$

C_b is Background count

T_b is Background Count Time

M_0 is Mass of standard

The calculation is part of the detector calculations. The background count was obtained by inserting an empty sample container with similar geometry to the containers used for the samples. The file containing the counting results of the background is accessed when analyzing the sample results in order to subtract background noise. The final sample results are net efficiency and net activity.

3.4 Determination of radiological effect

The following limits are recommended, UNSCEAR (2000)

i. Natural background dose rate: 2.5 mSv/hr
ii. Member of public dose rate limit : 1 mSv/hr
iii. Radiation worker dose rate limit : 20 mSv/hr
iv. Tissue reaction dose rate threshold : 1000 mSv/hr

3.4.1 Radium equivalent

This is a commonly used index to calculate activity concentrations of samples containing ^{226}Ra, ^{232}Th and ^{40}K. The assumption is that 10 Bq/kg of ^{226}Ra, 7 Bq/kg of ^{232}Th and 130 Bq/kg of ^{40}K will yield the same γ dose rate (Al-Trabulsy, 2010). The index is mathematically represented as,

$$Ra_{eq} = A_{Ra} + 1.43A_{Th} + 0.077A_K < 370 \quad (78)$$

Ra_{eq} is Radium equivalent activity, Bq/kg

A_{Ra} is activity of ^{226}Ra

A_{Th} is activity of ^{232}Th

A_K is activity of ^{40}K

The number 370 in equation 78 is equivalent to 1 mSv/y which meets the maximum permissible dose rate to members of the public.

3.4.2 Absorbed dose rate in air

The United Nations Scientific Committee on effects of atomic radiation, UNSCEAR, has adopted the absorbed dose rate as an indicator of ionizing radiation in the air 1 m above earth surface (El Afifi et al., 2006). The absorbed dose rate is represented by the following mathematical relation based on the UNSCEAR (2000) report.

$$D_\gamma = (0.462A_{Ra} + 0.604A_{Th} + 0.417A_K)\ x\ 10^{-3} \quad (79)$$

D_γ is $r$ate of dose from gamma rays, nGy/h

3.4.3 Annual Effective Dose Equivalent (AEDE)

The UNSCEAR (2000) report further proposes the following relation and its parameters to calculate the annual effective dose equivalent (El Afifi et al., 2006).

$$D_{eff} = D_\gamma\ x\ 10^{-3}\ x\ 8760\ x\ 0.2\ x\ 0.7 \quad (80)$$

D_{eff} is annual effective dose, mSv/y

Note:

$0.7\frac{Sv}{Gy}$: conversion of air absorbed dose rate to effective dose rate received by an adult

0.2: assumption that adults spend 20% of time outdoors

8760: number of hours per year

3.4.4 Hazard indices

Internal exposure Hazard Index:

$$H_{in} = \frac{A_U}{185} + \frac{A_{Th}}{259} + \frac{A_K}{4810} < 1 \quad (81)$$

External exposure Hazard Index:

$$H_{ex} = \frac{A_U}{370} + \frac{A_{Th}}{259} + \frac{A_K}{4810} < 1 \quad (82)$$

Data has been collected from different countries around the world in some oil industries. Typical ranges are shown in Table 11 below.

Table 11: Typical radiation risk indicators from some oil industries (Ali et al., 2019)

Country	Ra_{eq} (Bq/kg)	D_γ (nGy/h)	D_{eff} (mSv/y)
Saudi Arabia	21.6 - 204	10.5 - 96.4	0.013 - 0.118
Egypt	544 - 596	250 - 273	306 - 335
Tunisia	0.09 - 398	0.043 - 177	5.28×10^{-5} - 3.64×10^{-4}
Algeria		$(0.1 - 100) \times 10^3$	0.01 - 0.6
Nigeria	51.04 - 100.85	23 - 47	0.027 - 0.057
Congo	-	$(0.1 - 6) \times 10^3$	-
Italy	-	$(0.1 - 6) \times 10^3$	-
Ghana	-	10 - 57	12.6 - 83.4
USA	-	-	0.002 - 0.5

3.4.5 Estimated lifetime cancer risk

According to Mohammed (2017) the estimated lifetime cancer risk can be calculated using the following relation,

$$ELCR = AEDE_{out}\ x\ D_L\ x\ R_F \quad (83)$$

Where D_L is the period of life assumed to be 66 years and R_F is fatal risk factor per Sievert, 0.05 Sv^{-1}. They also stated that "1, 10, 100 and 1000 will cause an additional risk to develop a mortal cancer of 0.004, 0.04, 0.4 and 4% respectively".

4 Results and discussion

4.1 Identification of the radioactive nuclides

The nuclide identification is achieved by utilising the energy calibration curve. Counts are picked up in different channels. These channels represent energy peaks and these energy peaks in turn represent radioactive nuclides. As an illustration, the spectrum of samples D1S4, D1S12, D5S10 and D5S17 showed peaks at energy levels shown in Table 12 and Table 13 below. These energy peaks are signature gamma-ray energies for the particular radioactive nuclides and have been used to identify the corresponding radioactive nuclides.

Table 12: Identification of radioactive nuclides in samples D1S4 and D1S12

	Identified Nuclide	ID Confidence	Energy (keV)	Yield (%)	Activity (Bq/kg)	Activity uncertainty (Bq/kg)
Sample D1S4	K-40	0.969	1460.630	10.66	0.878	2.400
	Tl-208		583.190			
	Pb-210		46.54			
	Pb-212	0.899	238.632	43.60	0.535	0.189
	Bi-214	0.490	609.312	45.16	0.982	0.315
	Bi-214	0.490	1764.494	15.17	1.096	0.597
	Pb-214	0.785	295.224	18.28	0.021	0.370
	Pb-214	0.785	351.932	35.34	0.759	0.276
	Th-227	0.903	235.960	12.60	1.850	0.658
	Th-234	0.360	92.600	5.21	1.901	1.173
Sample D1S12	K-40	0.991	1460.630	10.66	0.000	0.000
	Tl-208	1.000	583.190	85.00	0.410	0.115
	Pb-210	1.000	46.54	4.25	19.120	4.210
	Pb-212	0.900	238.632	43.60	0.633	0.224
	Bi-214	0.500	609.312	45.16	0.842	0.238
	Bi-214	0.500	1764.494	15.17	0.079	0.749
	Pb-214	0.782	295.224	18.28	0.000	0.000
	Pb-214	0.782	351.932	35.34	0.828	0.467
	Th-227	0.895	235.960	12.60	2.190	0.783
	Th-234	0.358	92.600	5.21	1.314	0.900

Table 13: Identification of radioactive nuclides in samples D5S10 and D5S17

	Identified Nuclide	ID Confidence	Energy (keV)	Yield (%)	Activity (Bq/kg)	Activity uncertainty (Bq/kg)
Sample D5S10	K-40	0.999	1460.630	10.66	5.483	2.247
	Tl-208	1.000	583.190	85.00	0.665	0.141
	Pb-210	1.000	46.54	4.25	47.320	7.147
	Pb-212	0.901	238.632	43.60	1.159	0.289
	Bi-214	0.731	609.312	45.16	1.622	0.347
	Bi-214	0.731	1764.494	15.17	1.971	0.612
	Pb-214	0.786	295.224	18.28	1.576	0.489
	Pb-214	0.786	351.932	35.34	0.552	0.419
	Th-227	0.883	235.960	12.60	4.011	1.018
	Ac-228	0.496	270.240	3.55	6.256	2.422
	Ac-228	0.496	338.320	11.27	1.834	0.762
	Ac-228	0.496	911.200	25.80	1.478	0.655
	Th-234	0.360	92.600	5.21	1.901	1.173
Sample D5S17	K-40	0.993	1460.630	10.66	5.169	2.196
	Tl-208	0.998	583.190	85.00	0.371	0.184
	Pb-210	1.000	46.54	4.25	43.130	6.704
	Pb-212	0.900	238.632	43.60	1.325	0.086
	Bi-214	0.514	609.312	45.16	1.525	0.380
	Bi-214	0.514	1120.290	14.78	2.191	0.622
	Pb-214	0.999	295.224	18.28	1.186	0.497
	Pb-214	0.999	351.932	35.34	1.221	0.347
	Th-227	0.893	235.960	12.60	1.585	0.353
	Ac-228		270.240			
	Ac-228		338.320			
	Ac-228		911.200			
	Th-234	0.359	92.600	5.21	3.200	1.627

The presents of ^{40}K (1460.63 keV) has been confirmed in all samples. In the decay series of ^{238}U, the daughter nuclides ^{234}Th (92.6 keV), ^{214}Bi (609.312 keV), ^{214}Bi (1120.29 keV), ^{214}Pb (295.224 keV) and ^{214}Pb (351.932 keV) can be identified. In the decay series of ^{232}Th, the daughter nuclides ^{228}Ac (270.240 keV), ^{228}Ac (338.32 keV), ^{228}Ac (911.2 keV), ^{212}Pb (238.623 keV) and ^{208}Tl (583.19 keV) have been identified. Some of the radioactive nuclides did not appear in other samples.

4.2 Determination of individual nuclide activity concentration

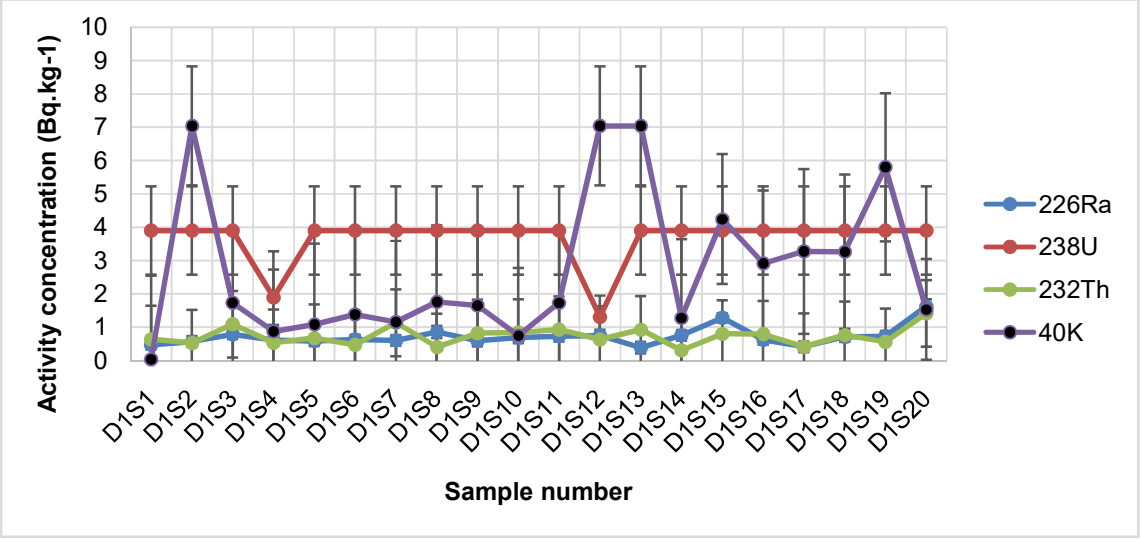

Figure 31: Activity concentrations of samples from the first drum

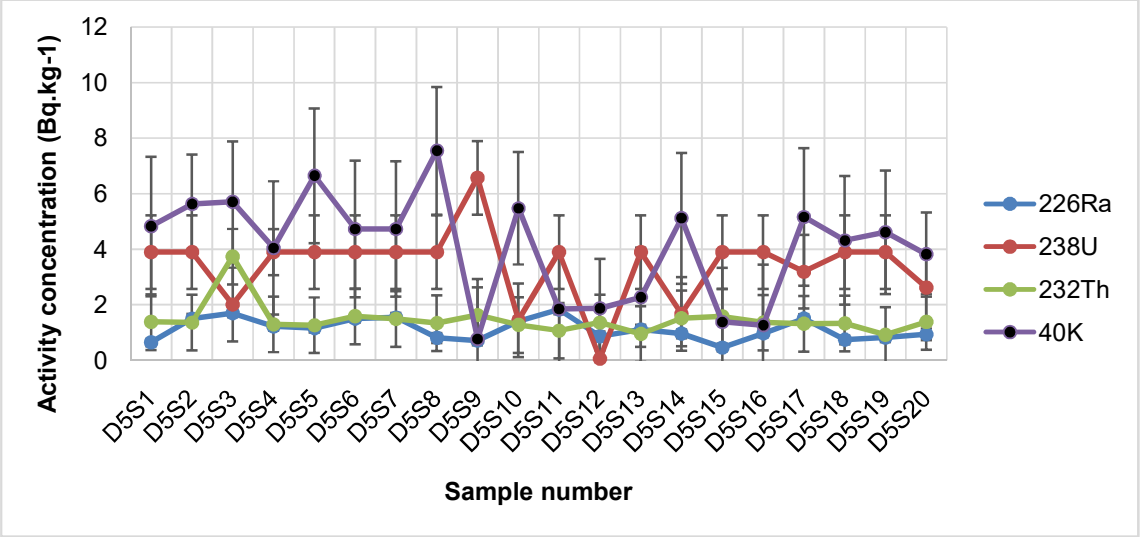

Figure 32: Activity concentrations of samples from the fifth drum

Weighted mean calculations were applied on activity concentration and activity concentration uncertainty results coming from Genie 2000 for all samples. The results are shown on Figure 31 for the first drum and Figure 32 for the second The weighted mean calculations for ^{238}U

were based on ^{234}Th (63.2 keV)) and ^{234}Th (92.6 keV). The weighted mean calculations for ^{232}Th were based on ^{212}Pb (238.632 keV); ^{228}Ac (33.32 keV) and ^{228}Ac (911.204 keV). The weighted mean calculations for ^{226}Ra were based on ^{214}PB (351.932 keV); ^{214}Pb (295.224 keV); ^{214}Bi (609.312 keV); ^{214}Bi (1120.287 keV) and ^{214}Bi (1764.494 keV). The results for ^{40}K and ^{210}Pb were used as is and no weighted mean calculation was done. The maximum, minimum and average values are shown in Table 14.

Table 14: Activity concentrations of NORM in scale

	Ra-226 (Bq/kg)		**U-238 (Bq/kg)**		**Th-232 (Bq/kg)**		**K-40 (Bq/kg)**		**Pb-210 (Bq/kg)**	
		Error, +/-		Error, +/-		Error, +/-		Error, +/-		Error, +/-
Max value	4.86	0.65	1.76	0.47	2.25	0.41	2.19	0.94	2.19	0.94
Min value	0.02	0.25	0.09	0.10	0.36	0.13	0.08	0.27	0.08	0.42
Average value	1.33	0.44	0.97	0.31	0.81	0.28	1.29	0.78	1.29	0.8

4.3 Comparisons nuclide activity concentration

Table 15: NORM activity concentration range for scale and deposits (IOGP, 2016a)

	NORM	(Bq/kg) [scale] x10^3	(Bq/kg) [deposit] x 10^3	**This study (Bq/kg)**
^{232}Th	^{232}Th	0.001- 0.002	0.001 - 0.07	0.36 – 2.25
	$^{228}Ra_{eq}$	0.05 - 2800	0.05 - 300	-
^{238}U	$^{238}U_{eq}$	0.001 - 0.5	0.001 - 0.05	0.09 – 1.76
	$^{226}Ra_{eq}$	0.1 - 15000	0.8 - 400	0.02 – 4.86
	$^{210}Pb_{eq}$	0.02 - 75	0.05 - 2000	0.08– 2.19

By comparing Table 14 and Table 15 it can be seen that the activity concentrations found in this study are far less than those recorded by (IOGP, 2016a) for both scale and deposit.

4.4 Estimation of the potential radiological risk

4.4.1 Radium equivalent

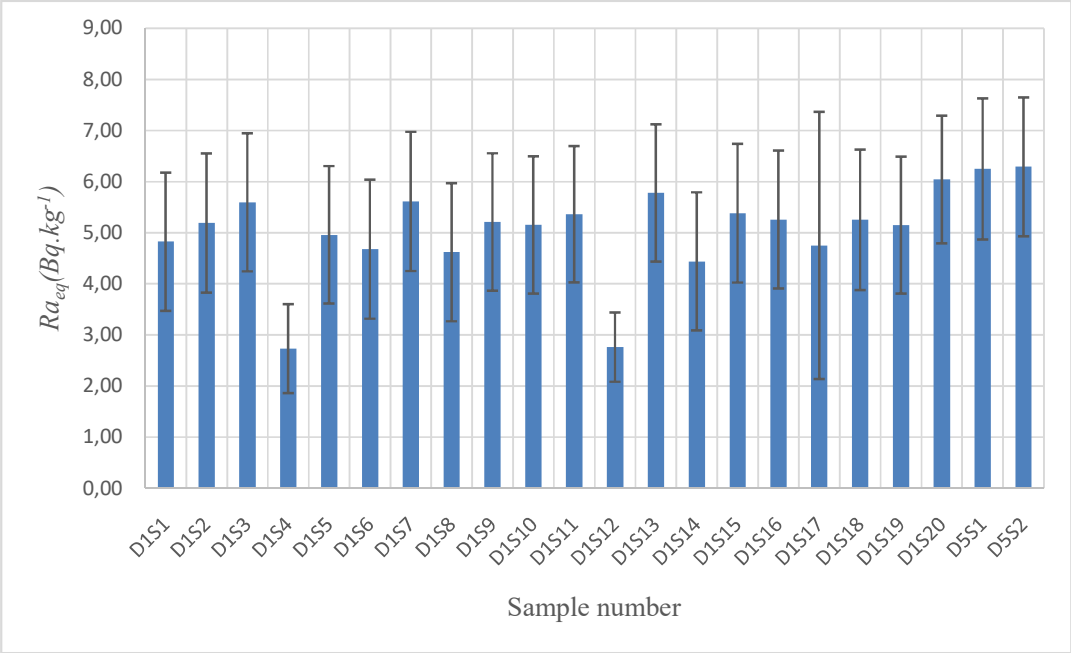

Figure 33: Radium equivalent for the first drum samples

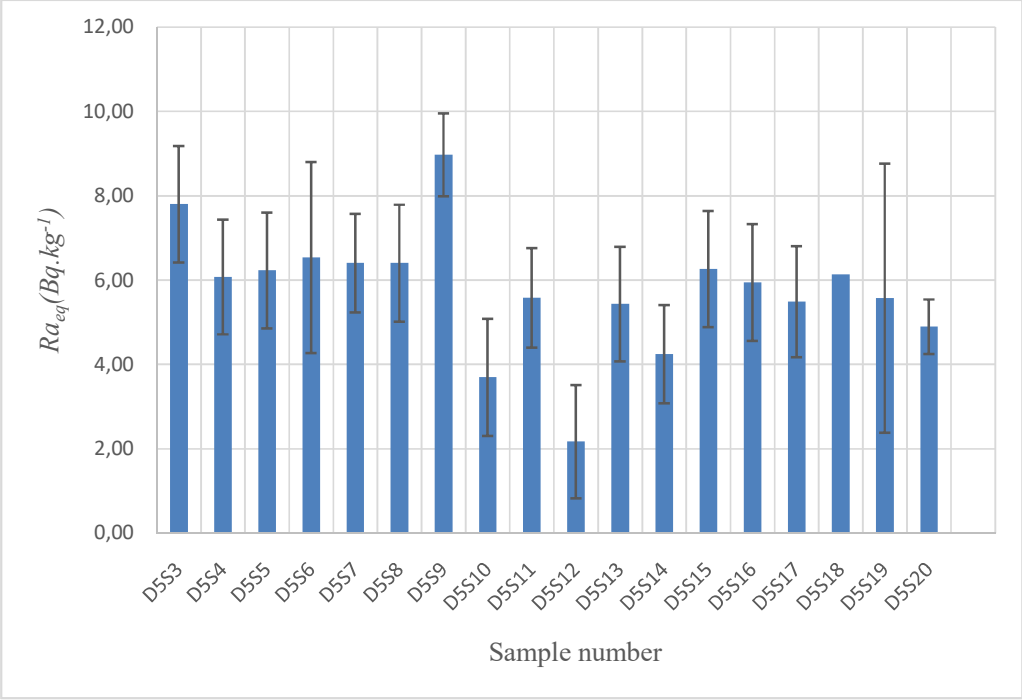

Figure 34: Radium equivalent for the fifth drum samples

The calculation of radium equivalent dose is based on equation 78 above. The results are shown on Figure 33 and Figure 34. The combined maximum, minimum and average values are in Table 16 below

Table 16: Results of Radium equivalent dose

	Ra (Bq/kg)	Error, +/-
Max value	8.98	3.19
Min value	2.17	0.00
Average value	5.39	1.35

The calculated radium equivalent in Table 16 is far less than 370 which is equivalent to 1 mSv/y which is the maximum permissible dose rate to members of the public. Therefore the maximum radium equivalent of 8.98 Bq/kg is far less than the maximum required for membes of the public.

4.4.2 Absorbed dose rate in air

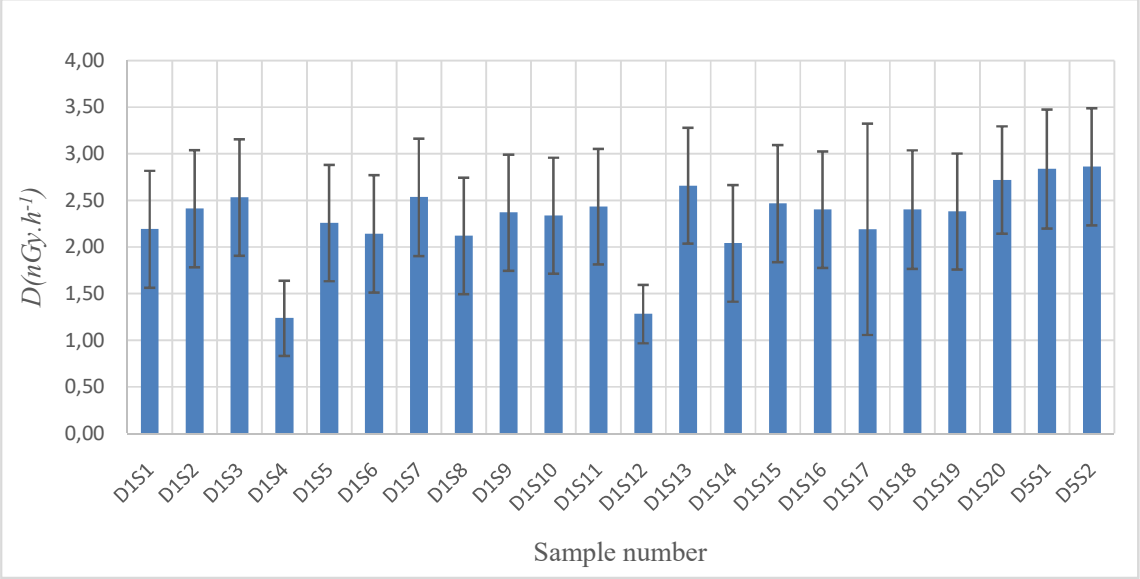

Figure 35: Absorbed dose for the first drum samples

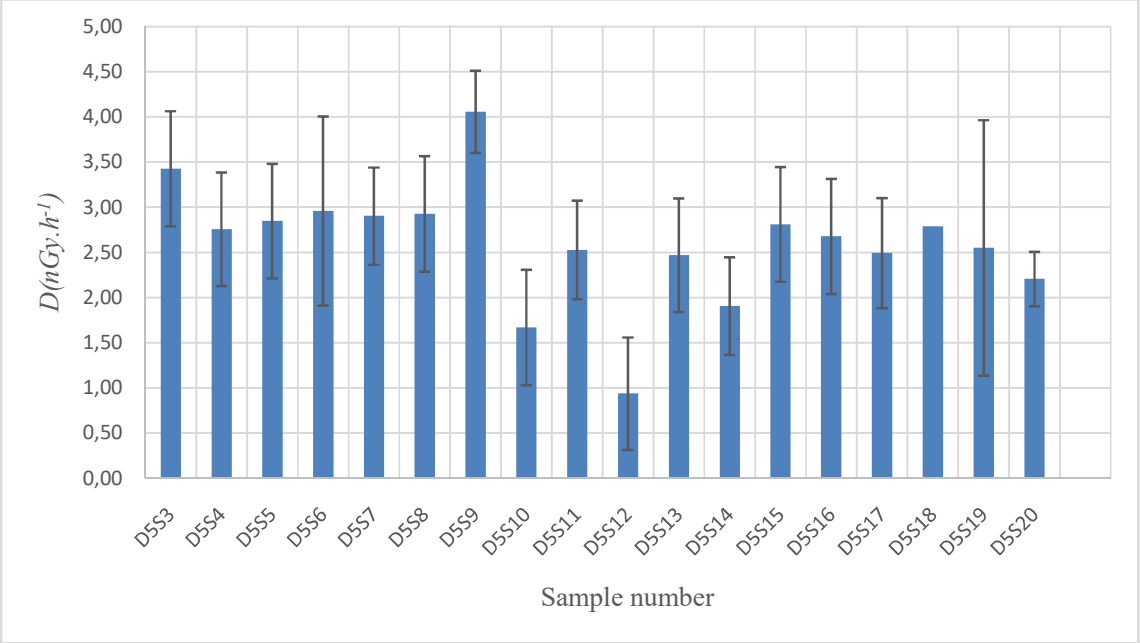

Figure 36: Absorbed dose for the fifth drum samples

The calculation of absorbed dose rate is based on equation 79 above. The results are shown on Figure 35 and Figure 36. The combined maximum, minimum and average values are in Table 17 below.

Table 17: Results of absorbed dose rate

	D (nGy/h)	Error, +/-
Max value	4.06	1.41
Min value	0.94	0.00
Average value	2.45	0.62

The recommended limit for total absorbed dose is 55nGy/h, El Afifi et al. (2006), for workers. The calculated total absorbed dose of 0.94 nGy/h is far less than the recommended value.

4.4.3 Annual Effective Dose Equivalent (AEDE)

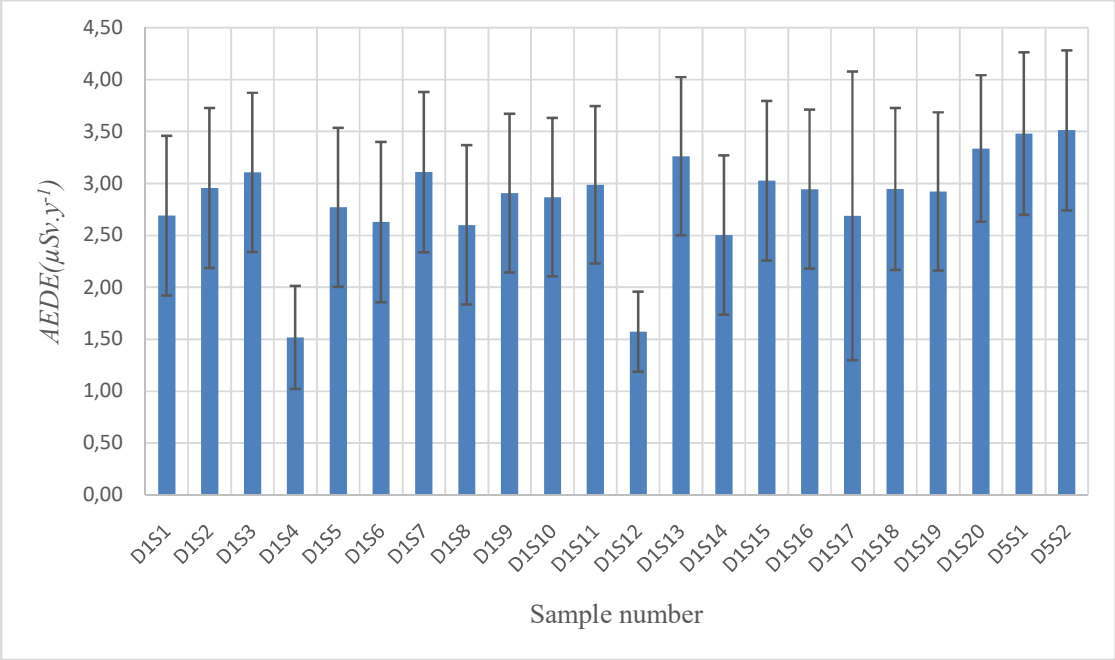

Figure 37: Annual effective dose equivalent for the first drum samples

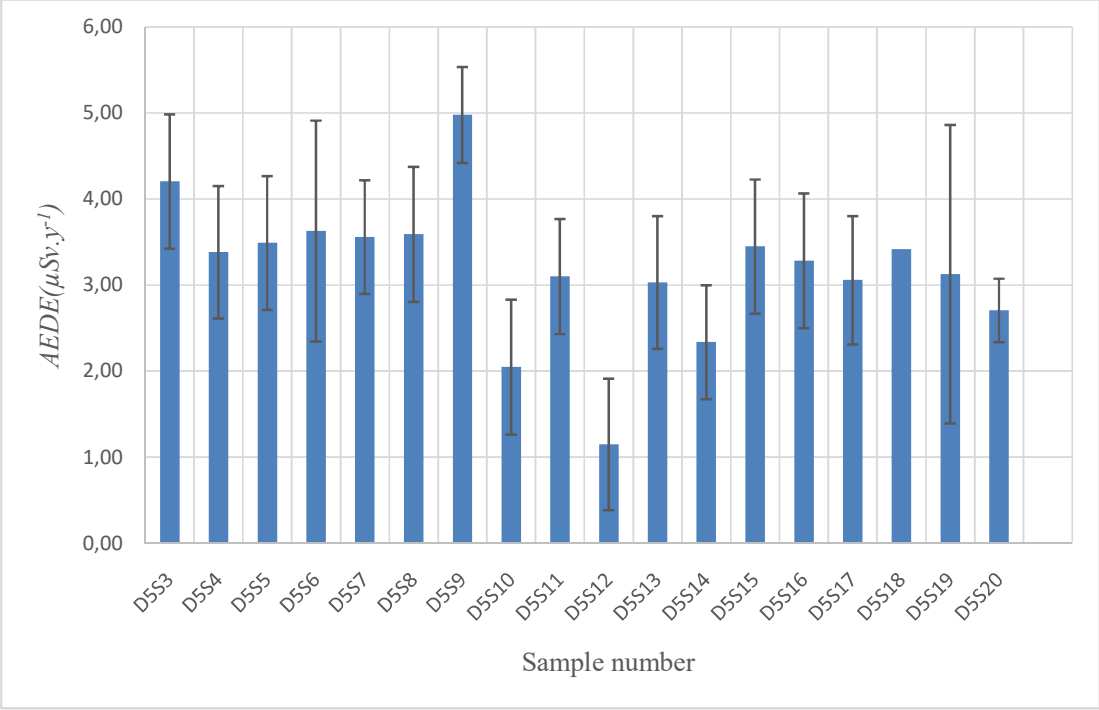

Figure 38: Annual effective dose equivalent for the fifth drum samples

The calculation of annual effective dose equivalent is based on equation 80 above. The results are shown on Figure 37 and Figure 38. The combined maximum, minimum and average values are in Table 18 below.

Table 18: Results of annual effective dose equivalent

	AEDE(μSv/y)	Error, +/-
Max value	4.98	1.74
Min value	1.15	0.00
Average value	3.01	0.76

The recommended annual effective dose equivalent is 70 μSv/y, UNSCEAR (2000). The maximum annual effective dose equivalent of 4.98 μSv/y is far less than the recommended value.

4.4.4 Comparison with other countries

Table 19: Comparison of radiological risks for this study with other countries

Country	Ra_{eq} (Bq/kg)	D_{γ} (nGy/h)	D_{eff} (mSv/y)
This study	**2.17-8.98**	**2.45-4.06**	**3.01-4.98**
Saudi Arabia	21.6 - 204	10.5 - 96.4	0.013 - 0.118
Egypt	544 - 596	250 - 273	306 - 335
Tunisia	0.09 - 398	0.043 - 177	5.28×10^{-5} - 3.64×10^{-4}
Algeria		$(0.1 - 100) \times 10^{3}$	0.01 - 0.6
Nigeria	51.04 - 100.85	23 - 47	0.027 - 0.057
Congo	-	$(0.1 - 6) \times 10^{3}$	-
Italy	-	$(0.1 - 6) \times 10^{3}$	-
Ghana	-	10 - 57	12.6 - 83.4
USA	-	-	0.002 - 0.5

Results of the radiological risks from this study compares well with those from other studies shown in Table 19 above. The results from this study are not only below recommended limits by UNSCEAR but compares favourably with other countries.

4.4.5 Hazard indices

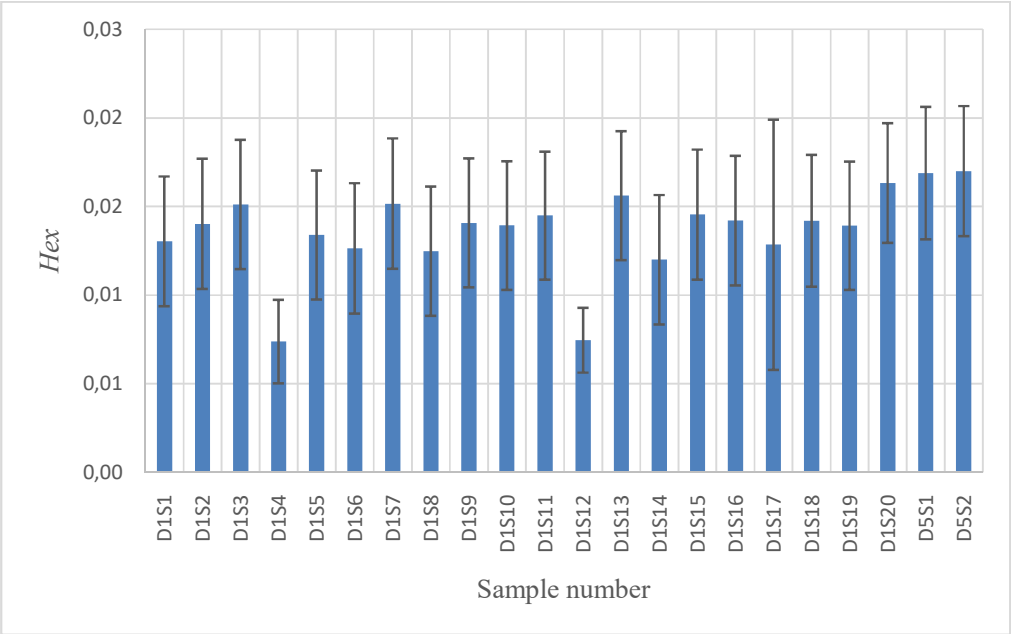

Figure 39: Hazard index for the first drum samples

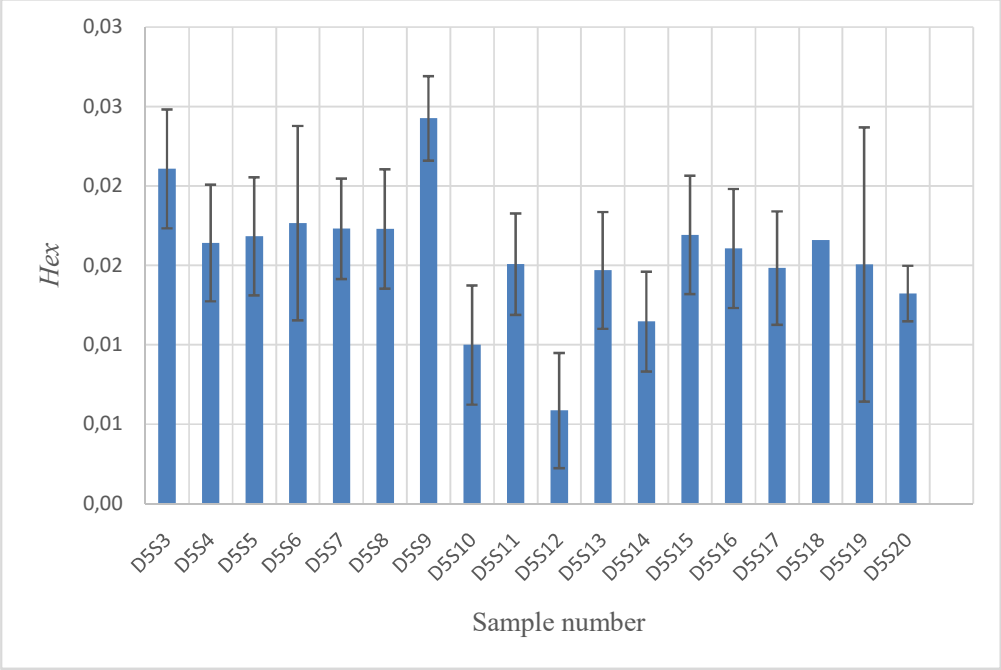

Figure 40 Hazard index for the fifth drum samples

The calculation of hazardous index is based on equation 82 above. The results are shown on Figure 39 and Figure 40. The combined maximum, minimum and average values are in Table 20 below

Table 20:Results of hazardous index

	Hex	Error, +/-
Max value	0.024	0.009
Min value	0.006	0,000
Average value	0.015	0.004

The hazard must be below 1 for the protection of personnel, UNSCEAR (2000). In this study the maximum is 0.024 and is far less than the recommended value.

4.4.6 Estimated lifetime cancer risk

The calculation of estimated life cancer risk is based on equation 83 above. The results are tabulated in Table 21 below

Table 21: Results of estimated life cancer risk

	ELCR x 10^{-3}
Max value	0.016
Min value	0.004
Average value	0.010

The maximum calculated estimation of life time cancer risk is 0.016 x 10-3. This is below world average according to Mohammed (2017) as shown in Table 22 below.

Table 22: Comparison of estimated lifetime cancer risk to world averages Mohammed (2017)

Study area	ELCR x 10^{-3}
This study	**0.016**
Nigeria	Negligible
Kerala, India	1.70
Kirklareli, Turkey	0.50
Azad Kashmir, Pakistan	2.17

4.5 Future work

In the topic proposal document it was mentioned that where possible, procedure for waste management and safe disposal would be looked at. However it has been agreed with the supervisor that the current work is enough. Developing waste management and disposal program is critical for this industry and especially in Southern Africa where natural gas exploration and production is still in its infancy. This could be work for the future.

The work done in this study is a snap shot based on samples from pipeline cleaning. Gas transportation using pipeline from Temane in Mozambique to Secunda in South Africa is just one section of a much bigger value chain. The value chain starts from the gas fields where gas is extracted from the gas wells as a mixture of gas, oil and water into the collecting lines and eventually gathered into the trunk lines to be transported to the gas processing plant. At the gas processing plant the gas goes through a three phase separator where the stream is separated into gas, oil condensate and produced water. Produced water is re-injected into old unused wells and the oil condensate is stabilised and taken to the markets. The gas is further purified taking out sour gas if present and dewatered and chilled to remove remaining oil before pressurised into the gas pipeline for transportation. This study has not been done at the gas fields and even at the gas processing plant. Herein lies an opportunity to do more work.

5 Conclusions and Recommendations

It can be concluded that NORM is present in the waste scale coming from the cleaning of the gas pipeline from Temane in Mozambique to Secunda in South Africa. The presence of ^{40}K, ^{232}Th and ^{238}U with their daughter nuclides has been confirmed with the use of the HPGe spectrometer. Each sample spectrum showed a peak at energy levels corresponding to radioactive nuclides in the thorium and uranium series and at the single energy level of potassium.

The activity concentration for each sample has been determined and it varies as shown in Table 14. This has been compared with industry values and has been found to be much less than the values in the industry as shown in Table 15. The maximum radium equivalent of 8,98 Bq/kg is far less than 370 Bq/kg which is equivalent to 1 mSv/y. From this study it is concluded that members of the public are not exposed to harmful radiation. The obtained radiation is far less than the 1 mSv/y which is the recommended limit for members of the public. The estimation of potential radiological risks based on radium equivilent, absorbed dose rate, annual effetive dose equivalent, hazard indices and estimated lifetime cancer risk shows that the workers and members of the public are not exposed to deterministic and stochastic health effects by being exposed to these levels of radiation.

It is recommended that this type of work must be done throughout the entire gas value chain starting from gas fields. Although the radiation activity concentration is low, the current commitment to strict safety procedures and high standards of protection of the public and environment be maintaned. It is further recommended that waste from pipeline scale be separated from contaminated safety clothes, gloves, filter catridges and any other contaminated articles. This will simplify disposal of all waste.

6 APPENDICES:

6.1 Calculated results

Sample ID	U-238 (Bq/kg)	Th-232 (Bq/kg)	K-40 (Bq/kg)	Absorbed Dose Rate (D) nGy/h	Radium Equivalent (Raeq) Bg/kg	AEDE (indoors) mSv/y	AEDE (outdoors) mSv/y	AEDE (external) mSv/y	Excess lifetime cancer risk $x10^{-3}$	Hazard indices (Hex)	Hazard indices (Hin)
D1S1	3.90	0.65	0.04	2.19	4.83	0.0108	0.0027	0.0134	0.0089	0.0130	0.0236
D1S2	3.90	0.52	7.04	2.41	5.19	0.0118	0.0030	0.0148	0.0098	0.0140	0.0246
D1S3	3.90	1.09	1.73	2.53	5.59	0.0124	0.0031	0.0155	0.0103	0.0151	0.0257
D1S4	1.90	0.53	0.88	1.24	2.73	0.0061	0.0015	0.0076	0.0050	0.0074	0.0125
D1S5	3.90	0.68	1.09	2.26	4.96	0.0111	0.0028	0.0139	0.0091	0.0134	0.0239
D1S6	3.90	0.47	1.38	2.14	4.68	0.0105	0.0026	0.0131	0.0087	0.0126	0.0232
D1S7	3.90	1.14	1.16	2.54	5.61	0.0124	0.0031	0.0156	0.0103	0.0152	0.0257
D1S8	3.90	0.41	1.76	2.12	4.62	0.0104	0.0026	0.0130	0.0086	0.0125	0.0230
D1S9	3.90	0.83	1.65	2.37	5.21	0.0116	0.0029	0.0145	0.0096	0.0141	0.0246
D1S10	3.90	0.84	0.75	2.34	5.15	0.0115	0.0029	0.0143	0.0095	0.0139	0.0245
D1S11	3.90	0.93	1.74	2.44	5.36	0.0120	0.0030	0.0149	0.0099	0.0145	0.0250
D1S12	1.31	0.63	7.04	1.29	2.76	0.0063	0.0016	0.0079	0.0052	0.0075	0.0110
D1S13	3.90	0.93	7.04	2.66	5.78	0.0131	0.0033	0.0163	0.0108	0.0156	0.0262
D1S14	3.90	0.31	1.29	2.04	4.44	0.0100	0.0025	0.0125	0.0083	0.0120	0.0225
D1S15	3.90	0.81	4.25	2.47	5.38	0.0121	0.0030	0.0151	0.0100	0.0145	0.0251
D1S16	3.90	0.79	2.91	2.40	5.26	0.0118	0.0029	0.0147	0.0097	0.0142	0.0247
D1S17	3.90	0.42	3.27	2.19	4.75	0.0108	0.0027	0.0134	0.0089	0.0128	0.0234
D1S18	3.90	0.77	3.27	2.40	5.25	0.0118	0.0029	0.0147	0.0097	0.0142	0.0247
D1S19	3.90	0.56	5.80	2.39	5.15	0.0117	0.0029	0.0146	0.0097	0.0139	0.0245
D1S20	3.90	1.42	1.54	2.72	6.04	0.0134	0.0033	0.0167	0.0110	0.0163	0.0269
D5S1	3.90	1.38	4.83	2.84	6.25	0.0139	0.0035	0.0174	0.0115	0.0169	0.0274
D5S2	3.90	1.37	5.63	2.87	6.29	0.0141	0.0035	0.0176	0.0116	0.0170	0.0275
D5S3	2.02	3.74	5.71	3.43	7.80	0.0168	0.0042	0.0210	0.0139	0.0211	0.0265
D5S4	3.90	1.30	4.05	2.76	6.08	0.0135	0.0034	0.0169	0.0112	0.0164	0.0270
D5S5	3.90	1.27	6.65	2.85	6.23	0.0140	0.0035	0.0175	0.0115	0.0168	0.0274
D5S6	3.90	1.59	4.74	2.96	6.54	0.0145	0.0036	0.0182	0.0120	0.0177	0.0282
D5S7	3.90	1.50	4.74	2.90	6.40	0.0142	0.0036	0.0178	0.0118	0.0173	0.0278
D5S8	3.90	1.34	7.55	2.93	6.40	0.0144	0.0036	0.0180	0.0119	0.0173	0.0278
D5S9	6.57	1.64	0.77	4.06	8.98	0.0199	0.0050	0.0249	0.0164	0.0243	0.0420
D5S10	1.45	1.28	5.48	1.67	3.70	0.0082	0.0021	0.0103	0.0068	0.0100	0.0139
D5S11	3.90	1.08	1.85	2.53	5.58	0.0124	0.0031	0.0155	0.0102	0.0151	0.0256
D5S12	0.07	1.37	1.88	0.94	2.17	0.0046	0.0012	0.0058	0.0038	0.0059	0.0061
D5S13	3.90	0.95	2.28	2.47	5.44	0.0121	0.0030	0.0152	0.0100	0.0147	0.0252
D5S14	1.68	1.52	5.12	1.91	4.25	0.0094	0.0023	0.0117	0.0077	0.0115	0.0160

D5S15	3.90	1.58	1.39	2.81	6.26	0.0138	0.0035	0.0173	0.0114	0.0169	0.0275
D5S16	3.90	1.36	1.27	2.68	5.95	0.0131	0.0033	0.0164	0.0108	0.0161	0.0266
D5S17	3.20	1.33	5.17	2.50	5.49	0.0122	0.0031	0.0153	0.0101	0.0148	0.0235
D5S18	3.90	1.33	4.33	2.79	6.14	0.0137	0.0034	0.0171	0.0113	0.0166	0.0271
D5S19	3.90	0.92	4.62	2.55	5.57	0.0125	0.0031	0.0157	0.0103	0.0151	0.0256
D5S20	2.62	1.39	3.82	2.21	4.90	0.0108	0.0027	0.0135	0.0089	0.0132	0.0203
Max value	6.57	3.74	7.55	4.06	8.98	0.02	0.00	0.02	0.016	0.02	0.04
Min value	0.07	0.31	0.04	0.94	2.17	0.00	0.00	0.01	0.004	0.01	0.01
Average value	3.54	1.10	3.44	2.45	5.38	0.01	0.00	0.01	0.010	0.01	0.02

7 References

AHMED, N. S. 2007. *Physics and Engineering of Radiation Detection*, Elsevier.

AL-TRABULSY, H. A. K., A.E.M; HABBANI, F.I 2010. Radioactivity levels and radiological hazard indices at the Saudi coastline of the Gulf of Aqaba. *Radiation Physics and Chemistry*.

ALI, M. M., ZHAO, H., LI, Z. & MAGLAS, N. N. 2019. Concentrations of TENORMs in the petroleum industry and their environmental and health effects. *RSC Advances,* 9**,** 39201-39229.

ATTALLAH, N. S. A., H.F 2012. Environmental Radioactivity of TE-NORM waste produced from Petroleum Industry in Egypt.

CAPP. 2018. *How smart pigs make pipeline safer* [Online]. Canadian Associstione of Petroleum Producers. Available: https://context.capp.ca/energy-matters/2018/em-og101how-smart-pigs-make-pipelines-safer/ [Accessed 2021].

ECKSTEIN, D. 2012. *RE: Solid State Detectors.*

EL AFIFI, E., HILAL, M., KHALIFA, S. & ALY, H. 2006. Evaluation of U, Th, K and emanated radon in some NORM and TENORM samples. *Radiation Measurements,* 41**,** 627-633.

EPCM. 2021. *PIPELINE PIGGING SYSTEM* [Online]. [Accessed 2021 URL Address https://epcmholdings.com/pipeline-pigging-system/].

FOLGA, S. M. 2007. Natural Gas Pipeline Technology Overview. Argonne National Laboratory.

HAZEN, R. M., EWING, R. C. & SVERJENSKY, D. A. 2009. Evolution of uranium and thorium minerals. *American Mineralogist,* 94**,** 1293-1311.

IOGP 2016a. Managing Naturally Occurring Radioactive Material in the Oil and Gas Industry. International Association of Oil and Gas Producers, Report 412.

IOGP, F. 2016b. Naturally Occurring Radioactive Material-The Facts.

JEVREMOVIC, T. 2009. *Nuclear Principles in Engineering*, Springer.

LAMARSH, J. R. B., ANTHONY.J 2001. *Introduction to Nuclear Engineering*.

LÉPY, M.-C. 2010. *RE: Detection efficiency.*

LIESER, K. H. 1997. *Nuclear and Radiochemistry: fundamentals and applications*.

MACMASTER, U. *Chapter 3 Gas Filled Detectors* [Online]. Medical Physics Dept. [Accessed 2021].

MACMASTER, U. *Chapter 4 Scintillation Detectors* [Online]. Medical Physics Dept. [Accessed 2021].

MACMASTER, U. *Chapter 8 Hyper-Pure Germinium Detector* [Online]. Medical Physics Dept. [Accessed 2021].

MIRION. 2020a. *HIGH-RESOLUTION GAMMA-RAY SPECTROSCOPY WITH HPGE DETECTORS* [Online]. [Accessed 2021 url address: https/www.mirion.com/learning-center/lab-experiments

].

MIRION. 2020b. *True Coincidence summing* [Online]. [Accessed 2021 url address: https/www.mirion.com/learning-center/lab-experiments].

MOHAMMED, R. S. A., R.S 2017. Estimation of excess lifetime cancer risk and radiation hazard indices in southern Iraq. *Environ Earth Science*.

MOKHATAB, S. M., D 2018. Liquefaction technology selection for baseload LNG plants. *Hudrocarbon Processing.*

NIKOLAOU, M., ECONOMIDES, M., WANG, X. & MARONGIU-PORCU, M. Distributed Compressed Natural Gas Sea Transport. Offshore Technology Conference, 2009. OnePetro.

NIKOLAOU, M. W., XIULI; ECONOMIDES, MICHAEL 2013. Optimization of compressed natural gas marine transportation with composite-material containers. *Society of Petroleum Engineers.* Jakarta, Indonesia.

PATAKI, G. E. & CAHILL, J. P. 1999. An investigation of naturally occurring radioactive materials (NORM) in oil and gas wells in New York State. *New York: Department of Environmental Conservation***,** 10-14.

PERSSON, H. 2019. Detection Limit Concepts According to Currie. Mirion Technologies: Mirion Technologies.

SANTAWAMAITRE, T. 2012. *An Evaluation of the Level of Naturally Occurring Radioactive Materials in Soil samples along the Chao Phraya River Basin.* PhD, University of Surrey.

THOMPSON, J. C., FRANK; FAHD, ZIAD; GAVITT, STEVE; GORETZKI, BRIAN; PATRICK, DALE 2015. Review of TENORM in the oil and gas industry. Conference of Radiation Control Program Directors, CRCPD E-15-2.

UNSCEAR 2000. SOURCES AND EFFECTS OF IONIZING RADIATION.

VAN DER WERFF, A. & BV, B. N. The importance of pipeline cleaning: risks, gains, benefits, peace of mind. Proceedings of the Pipeline Technology Conference, Hannover, Germany, 2006.

VAN ROOYEN, J. 2012. Transport and Shielding of Ionising Radiation. *Necsa. South Africa*.

VAN ROOYEN, J. 2020. Radiation Measurement, detection and instrumentation. *Lecture Notes.*

VAN ROOYEN, J. 2021. Radiation protection at Nuclear facilities: workers, Public and the environment. North-West University.

WALLBRINK, P., WALLING, D. & HE, Q. 2002. Radionuclide measurement using HPGe gamma spectrometry. *Handbook for the assessment of soil erosion and sedimentation using environmental radionuclides.* Springer.

WANG, L. & SUN, P. 2015. Long-distance Pipeline Pigging Technology. *International Journal of Science,* 2.

ZIELINSKI, R. A. & OTTON, J. K. 1999. *Naturally Occurring Radioactive Materials (NORM) in Produced Water and Oil-field Equipment: An Issue for Energy Industry*, US Department of the Interior, US Geological Survey.